Tellus (2008), 60A, 492–512
Printed in Singapore. All rights reserved

TELLUS

Aerosol-cloud-climate interactions in the climate model CAM-Oslo

By ALF KIRKEVÅG[1,2]*, TROND IVERSEN[1,2], ØYVIND SELAND[1,2], JENS BOLDINGH DEBERNARD[2], TRUDE STORELVMO[1] and JÓN EGILL KRISTJÁNSSON[1], [1]*Department of Geosciences, University of Oslo, P.O.Box 1022 Blindern, 0315 Oslo, Norway;* [2]*Norwegian Meteorological Institute, P.O.Box 43 Blindern, 0313 Oslo, Norway*

(Manuscript received 2 May 2007; in final form 8 January 2007)

ABSTRACT

A new aerosol module is integrated on-line in the atmospheric GCM CAM-Oslo coupled to a slab ocean for equilibrium climate response studies. The response to an anthropogenic change in aerosols since pre-industrial times is compared with that of a future 63% increased CO_2 level. The aerosol module calculates concentrations of sea-salt, mineral dust, sulphate, black carbon (BC) and particulate organic matter (POM). Look-up tables, constructed from first principles, are used to obtain optical parameters and cloud droplet numbers (CDNC) for any given aerosol composition. Anthropogenic aerosols thus produce a global near-surface cooling of 1.94 K and a 5.5% precipitation decrease, including amplifications by positive cloud feedbacks. In comparison, the CO_2 increase gives a warming of 1.98 K and a 3.8% precipitation increase, causing slightly reduced sulphate, BC, POM and sea-salt burdens. A minor increase in mineral dust is ascribed to reduced subtropical precipitation downwind of Sahara over the Atlantic Ocean. The modelled indirect effects are probably overestimated, mainly due to neglected natural aerosol components and the diagnostic scheme for CDNC. Adding 15cm^{-3} to CDNC everywhere reduces the indirect forcing from -2.34 to -1.36 Wm^{-2}, whilst solving a prognostic equation for CDNC reduces it from -2.34 to -1.44 Wm^{-2}.

1. Introduction

A global-scale warming of the earth's surface is now evident from observations. Increased concentrations of man-made greenhouse gases will continue to cause a significant global warming, even if greenhouse gas concentrations were to be stabilized (Teng et al., 2006; IPCC, 2007). However, uncertain cloud processes imply that the amplitude of the climate response to the anthropogenic external forcing is still uncertain (Murphy et al., 2004; Stainforth, et al., 2005; IPCC, 2007). The regional responses are even more uncertain as they may depend on strong non-local feedbacks (e.g. Boer and Yu, 2003). Furthermore, according to Andreae et al. (2005), the uncertainty regarding the cooling effect of aerosols is so large that our quantification of the climate sensitivity is highly uncertain mainly due to aerosols (see Fig. 2.20 in Forster et al., 2007). Even though the temperature change over the 20th century is well known, the corresponding net forcing is not. If the past aerosol forcing has been large, this implies a large climate sensitivity and a considerable risk for a stronger warming than anticipated from greenhouse gases alone in the 21st century.

Aerosols affect climate directly by reflecting and absorbing radiation, mainly in the short-wave. Indirect effects of aerosols are their altering of cloud properties such as the number and size of cloud droplets when activated as cloud condensation nuclei (CCN), or by changing the properties of cold clouds, for example, when serving as ice nuclei (see Lohmann and Feichter (2005) for a recent review). This paper attempts to increase the understanding of climate impacts of aerosols including interactions with greenhouse gas warming, using equilibrium climate response calculations with an atmospheric global climate model (GCM) extended with a new module for aerosols and coupled to a slab ocean.

Early published studies of the equilibrium climate response to the forcing of aerosols integrated on-line in GCMs, mainly discussed indirect aerosol effects (Rotstayn et al., 2000; Williams et al., 2001; Rotstayn and Lohmann, 2002). Qualitatively, they agreed on a substantial cooling at mid- and high-latitudes in the Northern Hemisphere and a southward shift of the Intertropical Convergence Zone (ITCZ) caused by a stronger cooling in the Northern Hemisphere (NH) than in the Southern Hemisphere (SH). The relatively strong cooling at high latitudes was a result of positive feedbacks with snow-cover and sea-ice (Williams et al., 2001). In Feichter et al. (2004), Takemura et al. (2005), Kristjánsson et al. (2005) and Kirkevåg et al. (2008), the

*Corresponding author.
e-mail: alf.kirkevag@met.no
DOI: 10.1111/j.1600-0870.2008.00313.x

response to the combined direct and indirect aerosol forcing was estimated. Also in these studies a southward shift of the ITCZ was found, although less pronounced by Feichter et al. (2004), using a more complex treatment of cloud droplet nucleation with reduced importance of sulphate aerosols compared to simpler schemes (cf. Lohmann and Feichter 2005; Penner et al., 2006; Storelvmo et al., 2006b).

In the AeroCom model intercomparison study by Schulz et al. (2006), the ensemble of results from nine different atmospheric global models yielded a global-mean direct aerosol forcing at the top of the atmosphere (TOA) of -0.22 W m^{-2}. The values ranged from -0.41 to $+0.04$ W m^{-2} for the individual ensemble members. In IPCC (2007) the TOA global radiative forcing due to the direct aerosol effect is reported in the range from -0.1 to -0.9 W m^{-2} with a best estimate of -0.5 W m^{-2}. The level of scientific understanding is characterized as low to medium. The estimated range of global indirect aerosol forcing in the same report is from -0.3 to -1.8 W m^{-2}, with a best estimate of -0.7 W m^{-2}. The level of scientific understanding is only slightly higher than in the third assessment report of IPCC (Ramaswamy, 2001). However, only the first indirect effect of an enhanced cloud albedo due to smaller and more numerous cloud droplets (Twomey, 1977) is considered by IPCC (2007).

The second indirect effect of increased cloud liquid water content (LWC) due to reduced autoconversion to precipitation when droplets become smaller (Albrecht, 1989), is still considered to be too uncertain scientifically to be quantified by IPCC. It has further been argued that this and similar secondary effects should be categorized as feedbacks. Recent estimates, including detailed cloud activation and aerosol treatments, tend to lie in a rather narrow range of -0.3 to -1.4 W m^{-2} (Lohmann and Feichter, 2005).

Even though these lower estimates compare better with satellite retrievals than higher estimates, the uncertainty is still large (Quaas et al., 2006; Storelvmo et al., 2006a). For instance, Lohmann et al. (2000) showed that a reduction of the background minimum number of cloud droplets from 40 to 10cm^{-3} led to an increased indirect aerosol effect from -1.1 to -1.9 W m^{-2} (Lohmann and Feichter, 2005). This minimum number is a surrogate for the pre-industrial background aerosol concentration, and is also discussed in the present work.

The main purpose of this paper is to estimate and study the climate response to forcing by anthropogenic aerosols since pre-industrial times, based on a fairly elaborate aerosol module in the atmospheric General Circulation Model (GCM) CAM-Oslo (Seland et al., 2008). We also calculate the response under CO_2-driven global warming, and thereby provide input for quantification of implied uncertainties in regional scenarios (Haugen and Iversen, 2008), including feedbacks of human-induced climate change on the spatial distribution of the aerosols. More specifically, we investigate the equilibrium climate response to forcing by anthropogenic aerosols, relative to pre-industrial time, and compare this response to that of a projected future increase of 63% in CO_2. Interdependencies between the effect of global warming and aerosols are also discussed.

The experimental tool is CAM-Oslo coupled to a slab ocean model. The aerosols included in the GCM interact with climate directly through reflection and absorption of short-wave radiation, and indirectly through their effects on cloud droplet number and size, which subsequently affect the release of precipitation in water clouds. As far as practically feasible with the present level of climate models and aerosol modelling, the aerosol life-cycling, the aerosol optical properties and the aerosols' interactions with cloud droplet number concentrations (CDNC) are based on internally consistent assumptions. Used in conjunction with observations the model calculations can be used for uncovering and reducing deficiencies or weaknesses in these assumptions. The relatively advanced status of the module for aerosols and their interactions with radiation and clouds lies mainly in two aspects: the online calculation of a natural background aerosol and the process-determined mixing state of the particles. Thus, there are a few more degrees of freedom compared to models with more presumptions about aerosol physics and composition. In this way, the module has a number of similarities with that of Stier et al. (2005), which has also been included in a fully coupled GCM (Stier et al., 2006) for transient climate response calculations.

CAM-Oslo includes important upgrades compared to the earlier CCM-Oslo (Iversen and Seland, 2002 and 2003; Kirkevåg and Iversen, 2002; Kristjánsson, 2002), which was also used for equilibrium climate response calculations (Kristjánsson et al., 2005; Kirkevåg et al., 2008), and was one out of three GCMs (Kirkevåg et al., 2005) which participated in the first phase of the AeroCom intercomparison (http://nansen.ipsl.jussieu.fr/AEROCOM/; Kinne et al., 2006; Textor et al., 2006; Schultz et al., 2006; Penner et al., 2006). Whilst the aerosols in CCM-Oslo included prescribed concentration fields for mineral and sea-salt aerosols and only one type of internal mixture, CAM-Oslo employs no prescribed aerosol types and describes a range of internal particle mixtures. The main formulations and qualities of the aerosol processes and properties in CAM-Oslo are thoroughly discussed in Seland et al. (2008), hereafter referred to with the abbreviation SIKS. As opposed to CCM-Oslo (Kirkevåg et al., 2005), the aerosol burdens in CAM-Oslo are not tuned to fit with optical depth retrievals from satellite instruments or any other observed data. We have used the emission fields given from the AeroCom project (Dentener et al., 2006) with only minor adjustments regarding the assumed initial particle sizes. This implies that there probably are missing contributions from, for example, non-desert mineral aerosols, particulate nitrate and possibly from particles of biological origins (Jaenicke, 2005; Leck and Bigg, 2007). Secondary organic matter produced from photochemical reactions is included in an approximate manner as direct emissions. Since hardly any GCMs presently treat these missing aerosols the way they should, we have chosen to highlight the consequences of these shortcomings directly

rather than hide them by further tuning or data constraining (e.g. Lohmann and Lesins, 2002; Cakmur et al., 2006; Quaas et al., 2006; Lohmann et al., 2007).

Consequences of a too thin natural aerosol contribution are to be expected in the results. We, therefore, present and discuss a tuning experiment in which a background aerosol is added. We also discuss the effects of the 'competition effect' when different types of hydrophilic aerosols are activated as CCNs and the supersaturation is reduced (Ghan et al., 1997 and 1998; Storelvmo et al., 2006b). However, these separate tests are made without coupling to the slab ocean and their climate response is therefore not discussed.

The next section gives a brief overview of the model tool with emphasis on the treatment of aerosols. Section 3 describes the setup for the model experiments. The main experimental results along with their interpretations are presented in section 4. Finally, section 5 contains a summary and the main conclusions.

2. The Model

In this study of equilibrium climate responses to anthropogenic aerosols and increased CO_2 levels, we apply CAM-Oslo coupled to a slab ocean model. CAM-Oslo (SIKS) is a modified version of the Community Atmosphere Model (CAM) version 3.0, developed at NCAR (Collins et al., 2006a), run at T42 spectral truncation and with 26 levels in the vertical. The modifications to CAM3 consist of: (a) Replacing the aerosol scheme in CAM3 with a more detailed aerosol scheme, including prognostic sulphate, particulate organic matter (POM), black carbon (BC), sea-salt and mineral aerosols; (b) Replacing the prescribed CDNC with diagnosed number concentrations of activated CCN, that is, aerosols larger than the critical radius for CCN-activation for any given chemical composition and supersaturation; (c) Retuning of parameters for formation of rain by autoconversion in the scheme for prognostic cloud water and (d) An adjustment of the cloud cover parametrization for cold (polar) clouds suggested by Vavrus (personal communication).

2.1. Use of look-up tables

Optical parameters and CDNC are calculated by use of pre-calculated look-up tables (see SIKS for full details). The table entries are calculated with a single air parcel model for a wide range of conditions determining size-distributed particle composition, and physical properties from Mie- and Köhler-theory. The physical properties are integrated over the aerosol size distributions for bulk properties.

Basis for the tables are size distributions for primary aerosols and nucleation mode particles assumed to be log-normally distributed initially, and then modified by internal mixing brought about by condensation and coagulation in clear and cloudy air, as well as wet-phase chemical processes in clouds. Modified size distributions and chemical compositions are then calculated for the air parcel using a sectional approachdescribed by Kirkevåg and Iversen (2002), with updates described by SIKS. The processes responsible for change in size distributions are condensation, coagulation, processes in clouds, and size-dependant deposition. The aerosols span radii from 0.001 to 20 μm, covering 44 discrete size classes with bin width $\Delta\log_{10}(r) = 0.1$. In CAM-Oslo's predecessor CCM-Oslo (e.g. Kirkevåg et al., 2008) only the prescribed sea-salt, mineral and a water soluble continental background aerosol were allowed to thus mix with sulphate, POM and BC. In CAM-Oslo also fine mode primary sulphate, POM and BC particles can mix with other substances by condensation and coagulation. At increasing relative humidity, hygroscopic aerosol particles, that is all particles except externally mixed BC, also grow by extracting water from unsaturated water vapour in the ambient air. CDNC are in CAM-Oslo determined from the aerosols diagnostically as the number concentrations of activated CCN.

The tables have been calculated for an array of entry values for ambient relative humidity (for optical properties) and supersaturation (for CCN concentrations) for each of the externally mixed aerosol modes, as well as for process tagged mass concentrations of internally mixed aerosols. During the integration of CAM-Oslo, values for bulk optical parameters and CCN-concentrations are obtained for arbitrary aerosol concentrations by interpolation between the pre-calculated tabulated values. This is done every time-step of 20 min for CCN concentrations, and every hour for aerosol optics (the radiation time-step). Entry points to the table interpolations relating to the internal mixing are concentrations from coagulation, condensation, and in-cloud processing. The applied interpolation methods and the parametrization of intermodal distribution of internally mixed mass are described in Kirkevåg and Iversen (2002) and Kirkevåg et al. (2005), with updates pertaining specifically to CAM-Oslo described in SIKS. See also the latter work for a more thorough description of the aerosol modes and physio-chemical processes treated in the model.

See Appendix for discussion of a recently discovered inaccuracy in the look-up tables described in SIKS.

2.2. Assumed supersaturations

The momentary realized supersaturation of water vapour is crucial for the determination of CCN activation. In reality, supersaturations depend on the speed of processes increasing the relative humidity and the efficiency of deposition of water vapour onto existing available surface area of water droplets and CCNs. Based on Abdul-Razzak and Ghan (2000), Storelvmo et al. (2006b) attempted to describe this process explicitly together with a prognostic equation for droplet number, using supersaturations based on a subgrid distribution of vertical velocities. This method is very recently also included in the present latest version of CAM-Oslo and used in a separate sensitivity test, see section 4.6. However, the main model runs are based on prescribed

values of supersaturation, which are grid-cell values used as input to the tables for CCN. With little direct observational basis, values are simply assumed to be 0.10% in stratiform clouds, 0.25% in convective clouds over ocean and 0.80% in convective clouds over land. A convective cloud is here defined as a cloud where the instantaneous convective precipitation exceeds 1 mm day^{-1}. This distinction follows Kristjánsson (2002), but the assumed supersaturations (Kirkevåg et al., 2005) are here considerably higher due to the generally smaller CDNC at a given supersaturation, especially in pristine environments. The applied supersaturations are still within the range of measured values in Pruppacher and Klett (1977). For a more detailed description of the aerosol and CDNC treatment in CAM-Oslo, see SIKS.

2.3. *On-line aerosols with feedbacks*

Apart from the differences in diagnostics (see section 3) compared to SIKS, the aerosols, as well as greenhouse gases, are here allowed to influence the modelled dynamics of the climate system, which again feed back on the spatial and temporal distribution of aerosols. The importance of these interactions has been studied by Iversen et al. (2005) and Kirkevåg et al. (2008) for CCM-Oslo, and is further discussed in section 4.4 for CAM-Oslo. As a consequence of running the model in this interactive mode, the simulated cloud liquid water path (LWP) is reduced considerably compared to CAM3. The LWP is linked to the tuning of the formation of rain by autoconversion in the scheme for prognostic cloud water, through the model simulated CDNC and effective cloud droplet radii. Using the same values as in the standard CAM3 for the parameters *critpr* (0.5 mm day^{-1}) and *r3lcrit* (10 μm), that is the critical precipitation rate due to enhanced collection efficiency and the critical radius for onset of autoconversion, respectively, the model produces a global mean LWP of about 81 g m^{-2}, compared to 122 g m^{-2} in CAM3 (Collins et al., 2006a). As shown in section 4.2, retuning *critpr* back to the CCM-Oslo value of 5.0 mm day^{-1} (Kristjánsson, 2002; Kristjánsson et al., 2005), and using *r3lcrit* = 15 μm (which is the value given in the CAM3 description by Collins et al., 2004, while 10 μm is used in the code), gives a LWP of 114 g m^{-2}, close to CAM3 as well as observed values.

2.4. *Adjustment for cold clouds*

The 'Freezedry' parametrization of polar cloud cover suggested by Steve Vavrus (personal communication) is a parametrization introduced to reduce the large positive biases in low cloud fractions in the Arctic in winter in CAM3. When the water vapour content is very low, much of the cloud water formed is assumed to freeze and precipitate. This 'Freezedry' parametrization of the stratiform cloud fraction may be expressed as

$$cl = cl_{\mathrm{orig}} \cdot [\max(0.15, \min(1.0, q/3.0)]\,,$$

where q is the specific humidity (in g/kg) and cl_{orig} is the original (diagnostic) stratiform cloud fraction in CAM3 (Boville et al., 2006). For a more detailed description of the scheme and more about the motivation for using it in CAM-Oslo, see SIKS. As shown in that work, aerosol column burdens and radiative effects are generally quite insensitive to the choice of stratiform cloud cover parametrization. For example, the change in global aerosol radiative forcing due to the 'Freezedry' parametrization was found to be about -0.01 and 0.02 W m^{-2} for the direct and the first indirect effect, respectively.

3. Experimental setup

The model is run with two sets of aerosol emissions and with two different CO_2 levels. The first two simulations are run with the 1990 ('present-day') CO_2 volume mixing ratio of 355ppmv (IPCC, 2001). We label the first experiment **somPre**, which is run with pre-industrial (1750) emissions of aerosols and aerosol precursors. The second experiment, the control simulation, **somB**, is run with present-day aerosol emissions. The present-day and pre-industrial emission strengths and injection heights (Dentener et al., 2006) are as recommended in the AeroCom intercomparison exercise (e.g. Schulz et al., 2006). However, as advocated by Seland et al. (2008), particle sizes at the point of emission have been modified somewhat for sea-salt, i.e. a 2% shift from coarse mode to accumulation mode particles. The third and last equilibrium simulation, **somBco2**, is run with present-day emissions for aerosols, but with a 63% increase in the CO_2 mass mixing ratio. While H_2O is a prognostic variable (as in CAM3), other greenhouse gases (CH_4, N_2O, O_3, CFC11 and CFC12) are kept at present-day levels in all the experiments.

The 63% increase from the 'present-day' CO_2 level of 355ppmv was originally chosen based on the following: In CCSM3 the transient climate response (TCR) for global surface air temperature at doubled CO_2, that is after 70 years simulation with 1% year^{-1} increase in CO_2, is about 1.48 K, while the equilibrium climate response (ECR) is estimated at 2.47 K (Kiehl et al., 2006). Assuming that the TCR/ECR surface air temperature ratio (of about 0.60) is the same in CAM-Oslo as in the host model, our equilibrium simulation should reach the same temperature as in the transient simulation in year 48 of the simulation. The CO_2 mass mixing ratio at this time is about 1.61 times the initial level. Adjusted towards a mean of about 20 other GCM CMIP2 runs (IPCC, 2001), we end up with a factor 1.63 increase compared to present-day (1990) levels, that is about 580 ppmv. With this approach we attempt, by use of equilibrium simulations, to find a rough estimate of the TCR at the time of doubling of CO_2 (after 70 years), assuming that the aerosol emissions remain approximately the same as at present. Since the ratio TCR/ECR in CAM-Oslo and CAM3 may be somewhat different, we only take the 63% increase as an approximation to the climate state after CO2-doubling in a CMIP2 experiment.

Each simulation is of 42-year duration, run with CAM-Oslo coupled to a slab ocean model. The coupling of CAM3 to a slab ocean model has been described in detail by Collins et al. (2004; 2006a). The open, that is, ice-free ocean component of the model consists of a prognostic equation for the ocean mixed layer temperature, subjected to fluxes to and from the atmosphere (F) and horizontal and vertical heat fluxes within the ocean (Q-flux). The ocean mixed layer depth is an annual average derived from the observational data by Levitus (1982), typically ranging between 10 and 30 m in the tropics and the high-latitude ice-covered regions, while at high latitudes otherwise the depths vary from 10 m to a specified cap of 200 m. To evaluate the ocean Q-flux, data for F derived from a control run with CAM, together with the seasonal cycle of sea surface temperature (SST) and sea ice are needed. A 30-year long simulation with the standard version of CAM3 driven by climatological, seasonally varying SST and sea ice concentration has been used for this purpose. Sea ice is calculated with the default sea ice module in CAM3, a pure thermodynamic model derived from the Community Sea Ice Model (CSIM, Briegleb et al., 2004).

After a spin-up period of about 15 years, the climate reaches a radiative quasi-equilibrium at the TOA with the given aerosol and CO_2 levels. Due to a non-physical error in the code, affecting the model output only, we have re-run the last 6 years of the 42-year simulations to obtain complete cloud forcing diagnostics. Unless specifically mentioned, the last 28 years have been used in the analysis for interpretation of climate equilibrium response. Estimated responses in temperature and precipitation have been subjected to a *t*-test (von Storch and Zwiers, 1999). Assuming that all the years are statistically independent, results which are not significant at the 95% level are shown as white patches in Fig. 8.

A difference from SIKS is that we in the present model setup take out fewer diagnostic variables in order to use a minimum of computational resources for the relatively long climate simulations. For example, true radiative forcings (requiring multiple calls of subroutines for radiative transfer) are not calculated. The aerosol treatment, including the spectral resolution used in the radiative transfer code, is the same as in SIKS, apart from the minor modification discussed in the Appendix. However, model output of aerosol optical depth (AOD), single scattering albedo (SSA) and asymmetry parameter, is in the present work taken out only for one wavelength band and only for the total aerosol, not for each compound. We use a relatively broad band in visible light, 0.35–0.64 μm, covering the most commonly measured wavelengths of 0.5 and 0.55 μm. Optical parameters in this band (vis) are Chandrasekhar averaged over a set of six narrower spectral bands (see SIKS) in the same way as in Kirkevåg and Iversen (2002). Denoting this aerosol optical depth AOD_{vis}, the globally averaged ratio $AOD_{vis}/AOD_{0.55\mu m}$ is about 1.03 in SIKS. Regionally it ranges between about 0.95 in areas with very large sea-salt aerosols around 60°S and up to about 1.18 over the most arid biomass burning areas in South America, where particle sizes are small. Over industrial areas in North America and Europe the ratio generally lies between 1.02 and 1.12, averaged over the year. For simplicity, AOD hereafter refers to AOD_{vis}, and SSA to SSA_{vis}.

Furthermore, the aerosol optical parameters are in this work calculated for daylight only, while in SIKS the output is averaged over both day and night values. Hence, intercomparisons of AOD or SSA between the two works are only approximate. In the control simulation (somB), globally averaged AOD and vertically integrated SSA amount to 0.128 and 0.965, see Table 1, compared to 0.143 and 0.963 in SIKS. More relevant

Table 1. Annually averaged global and hemispheric average of vertically integrated mass (burdens) for each prognostic constituent, the total aerosol optical depth (AOD ≡ AOD_{vis}), and the column integrated single scattering albedo, SSA, at visible wavelengths. The SSA is defined as 1 – ABS/AOD, where ABS is the absorption optical depth.

	SO_4 Burden (mg S m^{-2})	BC Burden (mg C m^{-2})	POM Burden (mg m^{-2})	Sea-salt Burden (mg m^{-2})	Dust Burden (mg m^{-2})	AOD	SSA
somPre							
Global	0.426	0.0514	1.238	10.26	18.46	0.091	0.983
NH	0.413	0.0523	1.278	7.09	34.43	0.086	0.976
SH	0.439	0.0504	1.197	13.44	2.49	0.096	0.990
somB							
Global	1.234	0.278	2.547	10.58	19.73	0.128	0.965
NH	1.723	0.339	2.639	7.47	37.01	0.143	0.954
SH	0.744	0.216	2.455	13.70	2.45	0.112	0.976
somBco2							
Global	1.227	0.274	2.515	10.31	19.88	0.126	0.965
NH	1.725	0.336	2.627	7.31	37.29	0.142	0.954
SH	0.728	0.211	2.404	13.31	2.48	0.110	0.976

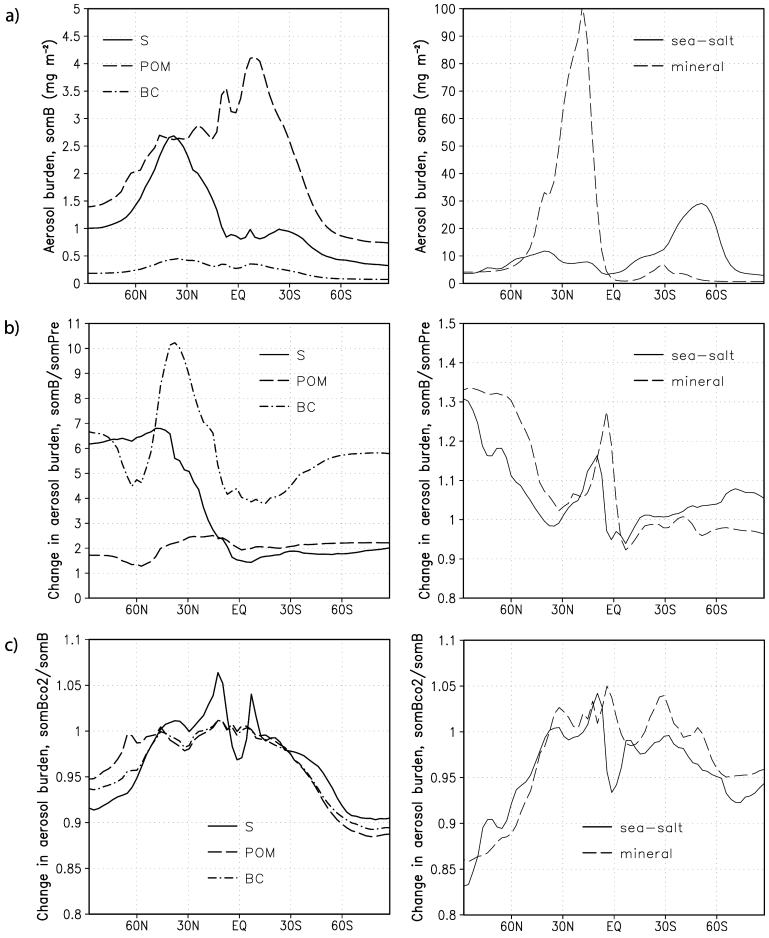

Fig. 1. Zonally averaged burdens (in mg m^{-2}) for sulphur (S), particulate organic matter (POM) and black carbon (BC) (left) and sea-salt and mineral aerosols (right), (a) With present-day emissions of aerosols and aerosol precursors (somB), (b) Relative change due to anthropogenic aerosols (somB divided by somPre), (c) Relative change due to a 63% increase in CO_2 (somBco2 divided by somB).

for the direct radiative forcing is the anthropogenic contribution to these optical parameters. In the present study, globally averaged anthropogenic AOD and SSA values (somB minus somPre) are about 0.037 and −0.018, respectively, close to the values of 0.037 and −0.015 in SIKS.

4. Results and discussion

4.1. Aerosol burdens, aerosol optical depths and cloud droplet properties

The main features of the horizontal distributions of aerosol burdens in the control simulation with present-day emissions of aerosols and aerosol precursors (somB) are similar to those discussed in SIKS, for an offline simulation with respect to aerosol-climate interactions. Due to different climates in the two simulations there are regional differences, however, resulting in somewhat reduced global aerosol burdens for sea-salt (−9%), dust (−3%) and sulphate (−4%), while BC (−0.1%) and POM (+0.2%) are almost unchanged compared to SIKS. Global and hemispheric averages of aerosol burdens are given in Table 1.

Regionally, the largest sulphate burdens are found over industrialized regions of North America, Europe, North Africa, South and East Asia, while POM generally has largest burdens in typical biomass burning regions, such as in South America, Africa and South-East Asia. The horizontal distribution of BC burdens is similar to that for POM, although a magnitude smaller and with relatively larger contributions from industrialized countries. Figure 1a shows zonally averaged aerosol burdens for sulphate (as Sulphur), POM, BC, sea-salt and mineral aerosols. Dust, or mineral burdens are particularly large over the desert areas, while sea-salt burdens have a maximum over southern parts of the Indian Ocean. Since both the mineral and sea-salt emissions are based on (fixed) climatological wind-fields and vegetation types etc., simulated changes in concentrations are entirely due to altered transport and deposition.

The relative change in aerosol burdens since pre-industrial time is shown in Fig. 1b. In spite of identical emissions of sea-salt and mineral aerosols in somPre and somB, climate responses to the direct and indirect effects of sulphate, POM and BC, cause significant changes in aerosol transport and deposition, which in turn yield somewhat larger sea-salt and mineral aerosol burdens at high latitudes. Similarly, when going from the somB to

somBco2 climate in Fig. 1c, the sulphate, POM and BC burdens are also distributed differently. This is partly a result of changed transport and deposition (no change in the emissions), but also due to changes in gas and wet-phase production of aerosols in the warmer climate. These effects are discussed in more detail in section 4.4.

The main features of the simulated all-sky AODs are also similar to those in SIKS, see Fig. 2a and Table 1, although there are regional differences and a 10% reduction globally, mainly due to reduced sea-salt burdens. AOD in the control simulation is estimated at 0.128 annually and globally averaged, with a dust-dominated maximum of about 0.55 over southern Sahara. Two other local maxima are 0.43 over north-eastern China, where anthropogenic aerosols dominate, and 0.28 over parts of the southern Indian Ocean, mainly due to sea-salt. Local maxima over North America and Europe are estimated at about 0.21 and 0.23, respectively. The anthropogenic contribution to the AOD, that is from simulation somB minus somPre, is about 0.037 globally averaged, see Table 1. From Fig. 2b we see that the maximum of about 0.35 is located over north-eastern China, where we also found the maximum for sulphate, as well as large BC and POM burdens. Local maxima over North America and Europe are both about 0.18. In southern Asia the anthropogenic AOD does not exceed 0.15, and over the biomass burning regions in Africa and South America, the annually averaged AOD due to human activity is estimated at less than 0.08 and 0.06, respectively. As discussed in SIKS, these anthropogenic optical depths are most likely underestimates. Globally averaged, modelled natural plus anthropogenic AODs in GCMs and Chemical Transport Models (CTMs) often lie in the range 0.06–0.15, which are at the lower end of estimates suggested by remote sensing from ground (AERONET, ca. 0.135) and space (satellite composite, ca. 0.15) (Kinne et al., 2006).

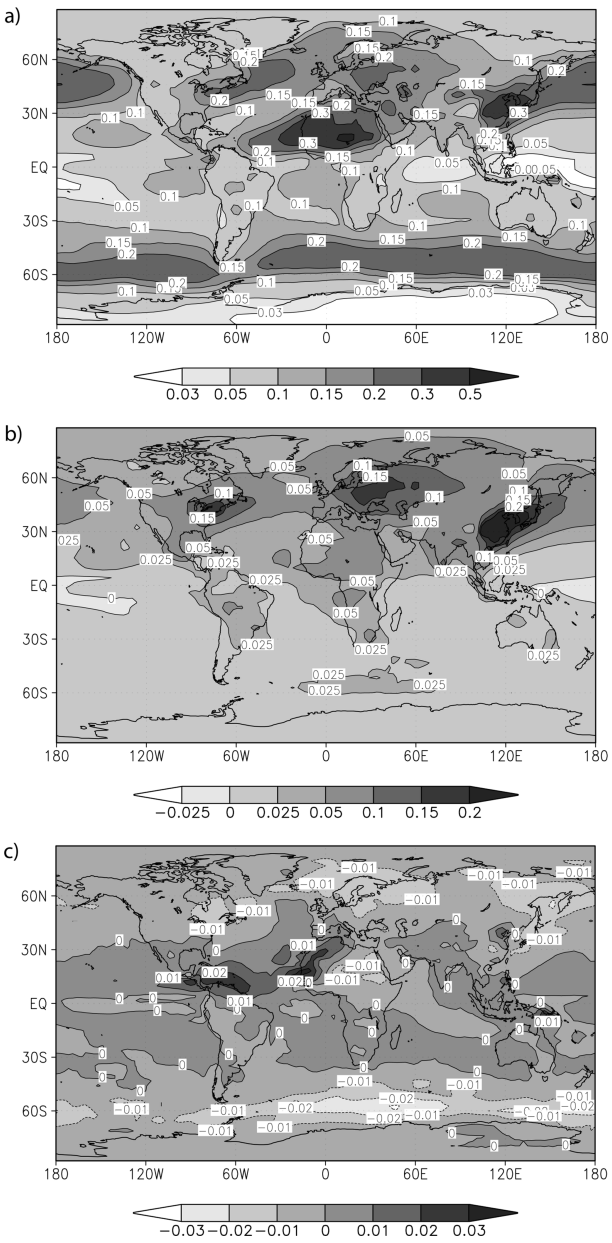

Fig. 2. Aerosol optical depth (AOD) in the wavelength band 0.35–0.64 μm, (a) With present-day emissions of aerosols and aerosol precursors (somB), (b) Change due to anthropogenic aerosols (somB minus somPre), (c) Change due to a 63% increase in CO_2 (somBco2 minus somB).

CDNC reflect concentrations of aerosol number and mass in competing measures, since sufficient size (as well as hygroscopicity) is necessary for CCN to activate, at the same time as the number of available aerosol particles represents an upper bound to the cloud droplet number. In some remote regions with small aerosol number concentrations and low supersaturations, the simulated CDNC may be as low as a few particles per cm^3. In the control simulation (somB) this is especially found to be the case in polar regions, but also over the southern oceans above about 850–900 hPa, see Fig. 3a. Apart from the very large simulated CDNC due to volcanic activity over New Guinea, the highest values are found over continental areas with large industrial or biomass burning emissions (see Seland et al., 2008). Compared to Kristjánsson (2002) the decrease in CDNC with height is quite small in many regions, and the CDNC even increases above about 700 hPa at mid- and high latitudes. This possibly counter-intuitive 'inversion' in cloud droplet numbers is a result of production of nucleation mode sulphate particles from clear-air oxidation of SO_2 under atmospheric conditions with little available surface area for condensation on pre-existing particles. The nucleated particles may further grow by condensation and coagulation to sizes large enough to produce cloud droplets (SIKS). A similar inversion for the nucleation of cloud droplets was found by Storelvmo et al. (2006b).

CDNC diagnostics are taken out only for temperatures above 0°C in the model. Hence, in Fig. 3 only the summer months contribute as high as up as 600 hPa at 60°N, with June standing out with the largest cloud droplet numbers, ca. 400 cm^{-3}. Averaging

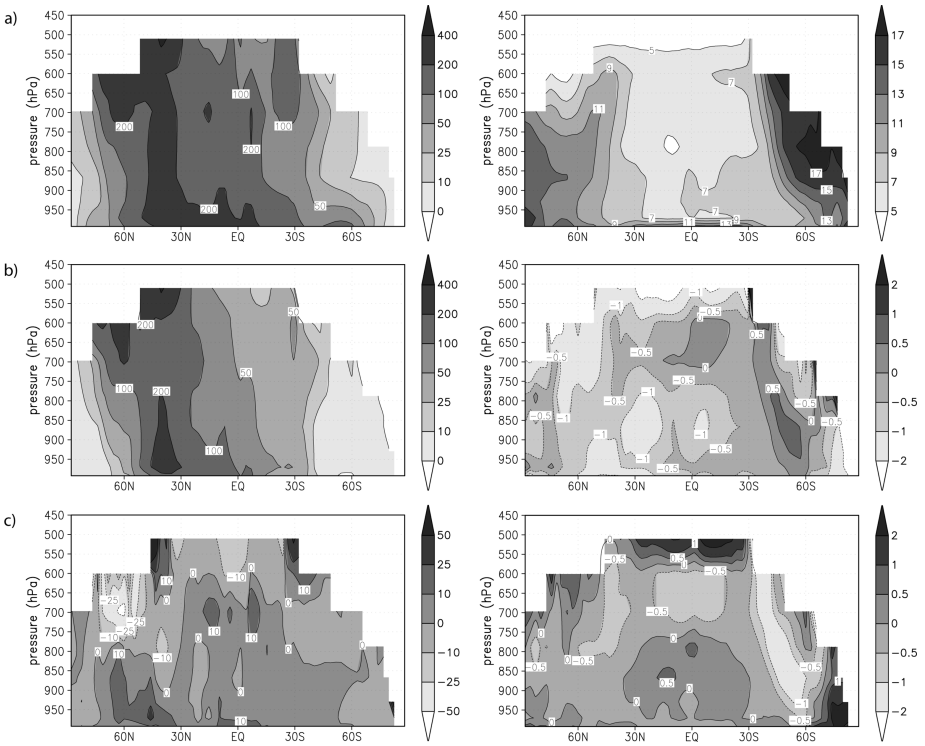

Fig. 3. Zonally and annually averaged cloud droplet number concentrations (left, in cm^{-3}) and cloud droplet effective radii (right, in μm), (a) With present-day emissions of aerosols and aerosol precursors (somB), (b) Change due to anthropogenic aerosols (somB minus somPre) (c) Change due to a 63% increase in CO_2 (somBco2 minus somB).

over time steps with non-zero CDNC, we find that up to 45% of the aerosol particles are here activated as CCN. Higher zonally averaged ratios of cloud droplet number to aerosol number (f_{ccn}) are only found immediately over the surface of the southern oceans, where accumulation mode sea-salt particles dominate. Assuming that the relative number fractions of the various aerosol particle modes are as in SIKS, the main contributors to the particle number concentrations are Aitken mode (70%) and nucleation mode (10%) sulphate, as well as an internally mixed Aitken mode of POM, BC and sulphate (10%). With a modal radius of 0.04 μm when emitted (SIKS), a rough estimate indicates that more than half of these particles will be activated under convective conditions with the assumed supersaturations. Continents cover most longitudes at 60°N, and monthly averaged convective precipitation over the continents indeed exceeds the threshold of 1 mm/day in June.

With a modal radius of 0.0118 μm for the nucleation mode sulphate, we estimate f_{ccn} to about 0.02 for $S_{ocean} = 0.25\%$ and 0.22 for $S_{continent} = 0.8\%$. With a monthly averaged mass mixing ratio of H_2SO_4 condensate of about 0.11 μg/kg produced by clear air oxidation, about three times as large as for the initial Aitken mode, we estimate condensation growth to yield f_{ccn} values of about 0.09 for $S_{ocean} = 0.25\%$, and 0.84 for $S_{continent} = 0.8\%$. Thus, for persistent convective conditions (with $S = 0.8\%$), more than two thirds of all particles could become activated CCN.

To summarize the large modelled f_{ccn} of about 0.45 aloft and the CDNC inversion at 60°N can be explained by the internally mixed Aitken mode sulphate aerosol, which itself exhibits an inversion with height both with respect to aerosol number concentrations and mass concentration of H_2SO_4 condensate. However, the assumed maximum supersaturation of 0.8% is probably an overestimate, given that the added sulphate is produced at higher levels than usually experience the maximum realization of supersaturation in convective clouds.

The effective liquid cloud droplet radius, R_{eff}, depends both on CDNC and in-cloud water content (e.g. Kristjánsson, 2002; Kristjánsson et al., 2005). Zonally averaged, R_{eff} in the control simulation has a minimum of about 5 μm at 750–800 hPa at about 10–15°N, see Fig. 3a, where LWCs are quite small. The largest droplet radii are found at high latitudes, with generally large LWC and small CDNC, especially over the southern oceans and into the Antarctica.

Comparing Fig. 3a with Fig. 3b, which shows the simulated increase in CDNC from pre-industrial time until today, we see that the majority of the cloud droplets at mid and high latitudes in the NH are from anthropogenic emissions, while in the SH a much larger contribution to CDNC comes from natural sources. Zonally averaged R_{eff} is reduced in large parts of the troposphere in both hemispheres, by up to as much as 2–3 μm at the highest altitudes where warm clouds can still be found. There are

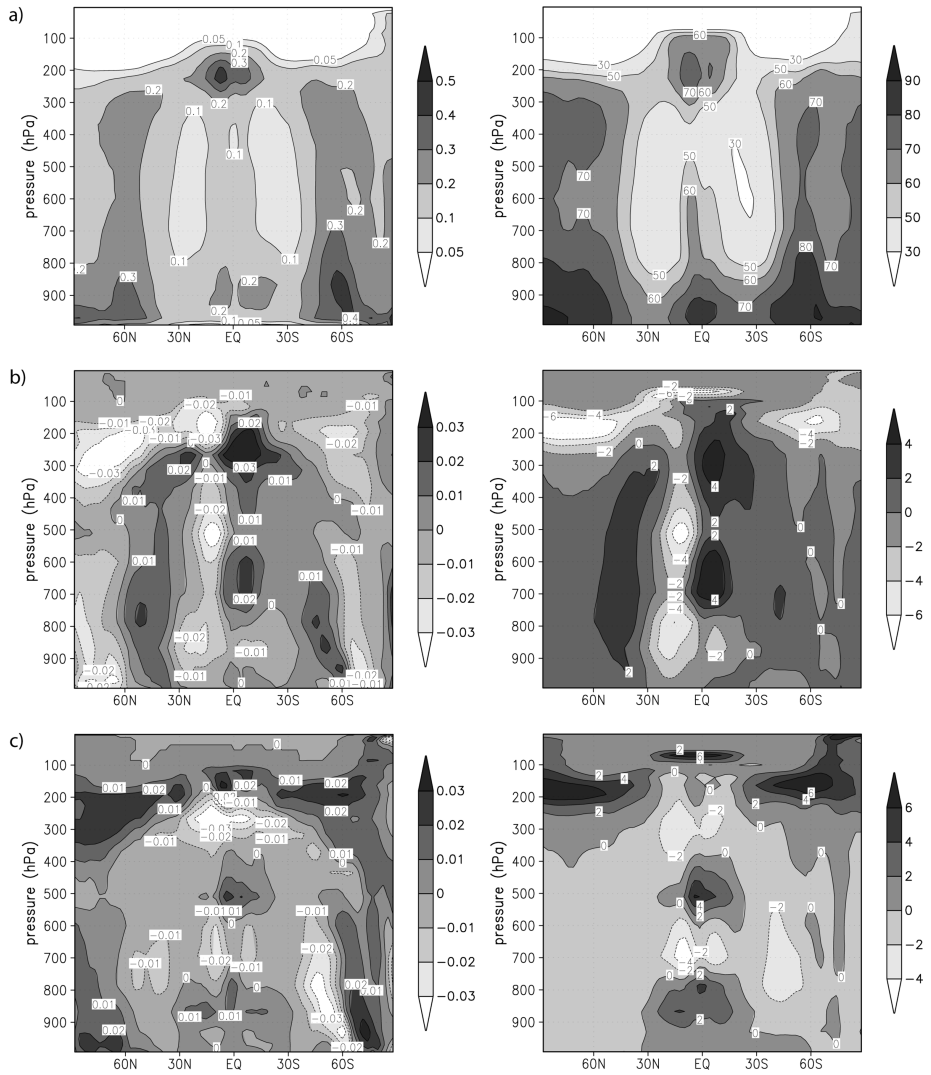

Fig. 4. Zonally and annually averaged cloud fraction (left) and relative humidity (%) (right), (a) With present-day emissions of aerosols and aerosol precursors (somB), (b) Change due to anthropogenic aerosols (somB minus somPre), (c) Change due to a 63% increase in CO_2 (somBco2 minus somB).

also significant changes in CDNC and R_{effl} between the somB and somBco2 simulations in Fig. 3c, which will be discussed in section 4.4.

4.2. *Simulation of present-day climate*

CAM-Oslo (coupled to a slab ocean) yields a quasi-equilibrium simulation of present-day climate, including observable parameters, such as cloud fields, precipitation, wind and surface air temperature. The 'Freezedry' parametrization of (cold) stratus clouds by Vavrus (Section 2.4) and the implemented aerosol module may influence the modelled climate compared to the original CAM3. As opposed to SIKS, who calculated meteorological fields online only with respect to the Vavrus scheme and the retuned autoconversion parameters, the present paper describes results of direct and indirect effects of aerosols calculated online with the meteorology and the slab ocean thermodynamics. We therefore have no explicit measure of the effect of the 'Freezedry' parametrization on cloud cover and cloud radiative forcing in the present CAM-Oslo version coupled to a slab ocean. The zonally averaged cloud cover as function of height is shown in Fig. 4a. In a test with the atmospheric CAM-Oslo presented in SIKS, the 'Freezedry' parametrization was shown to cause a reduction of 0.21 in the area averaged low cloud fraction north of 70°N and 0.13 south of 70°S. The respective reductions in total cloud cover were 0.17 and 0.09, and the short-wave cloud forcing (SWCF) decreased in absolute value by about 0.3 W m^{-2} and 0.5 W m^{-2} in the two regions, respectively. This implied only a slightly weakened short-wave cooling, but a reduced long-wave cloud forcing (LWCF) of about 1.8 W m^{-2} north of 70°N and

Table 2. Global and hemispheric annual means of surface air temperature, sea-ice area, precipitation and cloud liquid and ice water paths. Surface air temperature is defined as the temperature at reference height in the model (2 m above the ground over land).

	Surface air temperature (°C)	Precipitation (mm /day)		Cloud Cover (%)	Cloud Liquid Water Path (g m^{-2})	Cloud Ice Water Path (g m^{-2})	Sea-Ice Area (10^6 km^2)
		Total	Stratifotm				
somPre							
Global	17.40	3.10	0.737	60.8	106.3	14.53	9.25
NH	18.73	3.39	0.684	61.6	107.3	14.31	6.59
SH	16.08	2.82	0.791	60.0	105.2	14.75	2.66
somB							
Global	15.47	2.93	0.732	60.3	113.7	15.61	12.44
NH	16.20	3.01	0.676	60.3	118.2	15.58	8.01
SH	14.74	2.85	0.788	60.2	109.1	15.64	4.43
somBco2							
Global	17.45	3.04	0.729	60.9	115.3	14.82	8.67
NH	18.15	3.11	0.676	61.1	120.4	14.72	6.87
SH	16.76	2.98	0.782	60.7	110.3	14.93	1.80

Table 3. Global annual mean climatological properties of CAM-Oslo (somB), compared with CAM3 (Collins et al., 2006a) and observations. FK06 refers to Fetterer and Knowles (2002, updated 2006), and LW90 to Legates and Willmott (1990). C06 refers to observation data compiled by Collins et al. (2006a).

Quantity (units, observational source)	Observations	CAM3	CAM-Oslo
TOA short-wave cloud forcing (W m^{-2}, C06)	−54.2	−54.7	−53.7
TOA long-wave cloud forcing (W m^{-2}, C06)	30.4	30.7	29.4
Total cloud fraction (%, C06)	66.7	56.1	60.3
Cloud water path (g m^{-2}, C06)	112	122	114
Precipitation (mm day^{-1}, C06)	2.61 – 3.1	2.87	2.93
Latent heat flux (W m^{-2}, C06)	84.9	83.8	84.9
Sensible heat flux (W m^{-2}, C06)	15.8	17.8	19.1
Net surface long-wave radiation (W m^{-2}, C06):			
All-sky	49.4	58.0	58.0
Clear-sky	78.7	85.8	85.6
Net surface short-wave radiation (W m^{-2}, C06):			
All-sky	165.9	159.1	163.3
Clear-sky	218.6	218.6	220.9
Surface air temperature (K, LW90)	287.6	287.3	288.6
Sea-Ice Area (10^6 km^2, FK06)	18.6		12.4

0.7 W m^{-2} south of 70°S. Hence the 'Freezedry' parametrization causes a net radiative cooling by clouds in the Arctic of about −1.4 W m^{-2} north of 70°N in CAM-Oslo. A small effect is also found in the Antarctica: −0.2 W m^{-2} south of 70°S.

Despite this cooling effect, surface air temperatures are too high with the present model set-up. Comparing observed surface air temperatures over land with the IPCC/CRU 1961–1990 climatology (see http://www.ccsm.ucar.edu/models/atm-cam/sims/cam3.0), CAM-Oslo produces reasonable temperatures in the tropics (within about 1 K), but a warm bias for mid- and high-latitudes, with a regional maximum of about 10 K in the Arctic. Globally averaged surface air temperature is 15.5°C (Table 2) in the control simulation, compared to 14.1°C in CAM3, see Table 3. A preliminary simulations without the retuning of the autoconversion parameters described in section 2.3 resulted in a even larger warm bias. This warm bias globally could have been reduced by using CAM-Oslo instead of the original CAM3 for evaluating the ocean heat transport fluxes (the Q-flux term, cf. section 3) which are presently being used. This alternative approach would have minimized the difference in mean climate between CAM-Oslo and CAM3, but was hampered by limited time and computational resources. This alternative will be investigated in future work.

As a result of overestimated surface air temperatures, we underestimate sea-ice fractions and thus also the sea-ice area (see Tables 2 and 3), especially in the summer season. Furthermore,

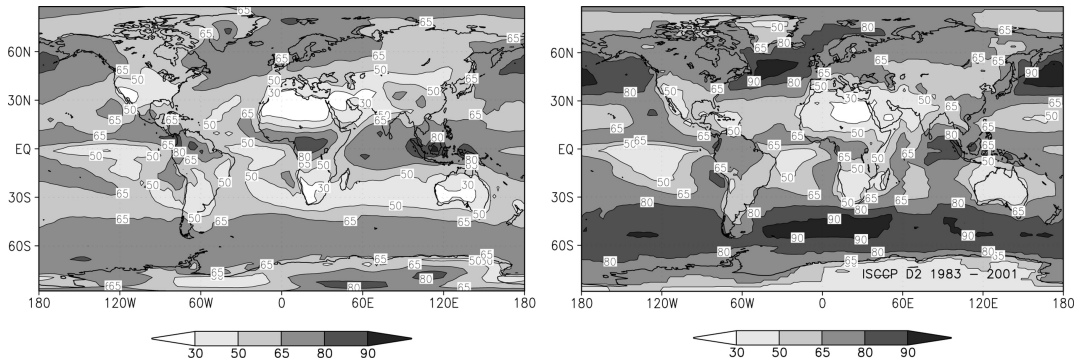

Fig. 5. Total cloud cover (%) in the control simulation somB to the left, and in the International Satellite Cloud Climatology Project data (ISCCP D2, July 1983 to June 2001) to the right.

precipitation rates are somewhat large. Globally averaged precipitation is estimated at 2.93 mm day^{-1}, while CAM3 produces 2.83 mm day^{-1} (Collins et al., 2006a). Observation-based values vary, from 2.61 mm day^{-1} in the GPCP 1979–2002 data, to 3.12 mm day^{-1} in the Legates and Willmott 1920–1980 data, see Table 3, but the simulated precipitation is most likely an overestimate for present-day climate.

Globally averaged total cloud cover is estimated at 0.603 in the control simulation, about midway between 0.561 in CAM3 (Collins et al., 2006a) and 0.667 in the International Satellite Cloud Climatology Project estimates (ISCCP, Rossow and Dueñas, 2004), see Tables 2 and 3. Comparing zonally averaged values with Hack et al. (2006), we find that the cloud cover in CAM-Oslo is generally larger than in CAM3 at mid-latitudes (especially in the NH) and in the tropics, in somewhat better agreement with ISCCP. An observed local maximum a few degrees south of the equator is reproduced in our control simulation, while the local minima in the subtropics are dislocated by about 10° polewards, as in CAM3. Despite the improvement at mid-latitudes, the regional picture in Fig. 5 shows that CAM-Oslo underpredicts the cloud cover at about 50° of latitude in both hemispheres. Another feature that stands out is the excessive cloud cover in the western Indian Ocean, as in CAM3. Arctic cloud fractions in both CAM-Oslo and CAM3 compare decently to ISCCP. However, the ISCCP data are not very reliable over snow and ice covered areas (Rossow and Schiffer, 1999).

In CAM3 prescribed CDNC concentrations are applied for calculation of effective droplet radii used in the prognostic cloud water scheme, and independently prescribed effective droplet radii for calculations of short-wave scattering by the droplets and for deposition velocities (Boville et al., 2006). When coupling these variables to the aerosol schemes in a more internally consistent manner as in CAM-Oslo, there is obviously less room for tuning. After adjusting the two parameters for autoconversion as described in section 2.3, the globally averaged LWP is estimated at 114 g m^{-2} (Table 2), close to the 112 g m^{-2} retrieved from MODIS and the 122 g m^{-2} in CAM3 (Collins et al., 2006a), see Table 3. In the extratropical storm tracks, LWP in CAM3 and CCSM3 is approximately twice as large as observed (Hack et al., 2006). Comparing zonally averaged LWP over ocean with that work, we see that the overestimate at mid-latitudes in our control simulation is significantly smaller, and in the Arctic we obtain LWP values of about 150 g m^{-2}, quite close to the values from the MODIS retrieval. Figure 6a shows regional LWP produced in our control simulation. In the tropics the LWP is considerably lower than in CAM3 and CCSM3, which is an improvement compared both with MODIS and the NASA Water Vapour Project global water vapour dataset (NVAP), but not compared to the data from the Special Sensor Microwave/Imager (SSM/I) (Hack et al., 2006). Simulated IWP is quite close to CAM3 (Hack et al., 2006) in the Arctic and in the Antarctica, but lower by about 5 and 5–10 g m^{-2} at low- and mid-latitudes, respectively.

Globally averaged, the short-wave cloud forcing (SWCF) is estimated at −53.7 W m^{-2}, see Tables 3 and 4, close to the −54.1 W m^{-2} from Earth Radiation Budget Experiment (ERBE) (Harrison et al., 1990; Kiehl and Trenberth, 1997) as well as to −54.7 W m^{-2} in CAM3 (Collins et al., 2006a) and −54.0 W m^{-2} in CCSM3 (Collins et al., 2006b). Comparing zonally averaged SWCF with Collins et al. 2006b), we find that CAM-Oslo has somewhat better agreement with ERBE than CCSM3 in the tropics and at mid-latitudes in the SH, while the agreement is somewhat poorer at high latitudes in the NH. In the Arctic the SWCF bias is up to about −18 W m^{-2}, about −2 W m^{-2} stronger than in CCSM3. Some of this bias may be due to the warm bias in the Arctic, however, giving spuriously small sea-ice fractions and surface albedo. Figure 7a confirms the agreement between simulated SWCF and ERBE data at mid-latitudes also regionally. In spite of a generally good agreement for the zonally averaged SWCF in the tropics and SH mid-latitudes, there are larger regional discrepancies, for example over the equatorial Pacific and Indian Oceans, and over tropical South America, where the simulated SWCF is too small. The excessive cloud cover, LWP and precipitation, and in turn also the cloud forcing over the western Indian Ocean are related to deficiencies in the Zhang McFarlane

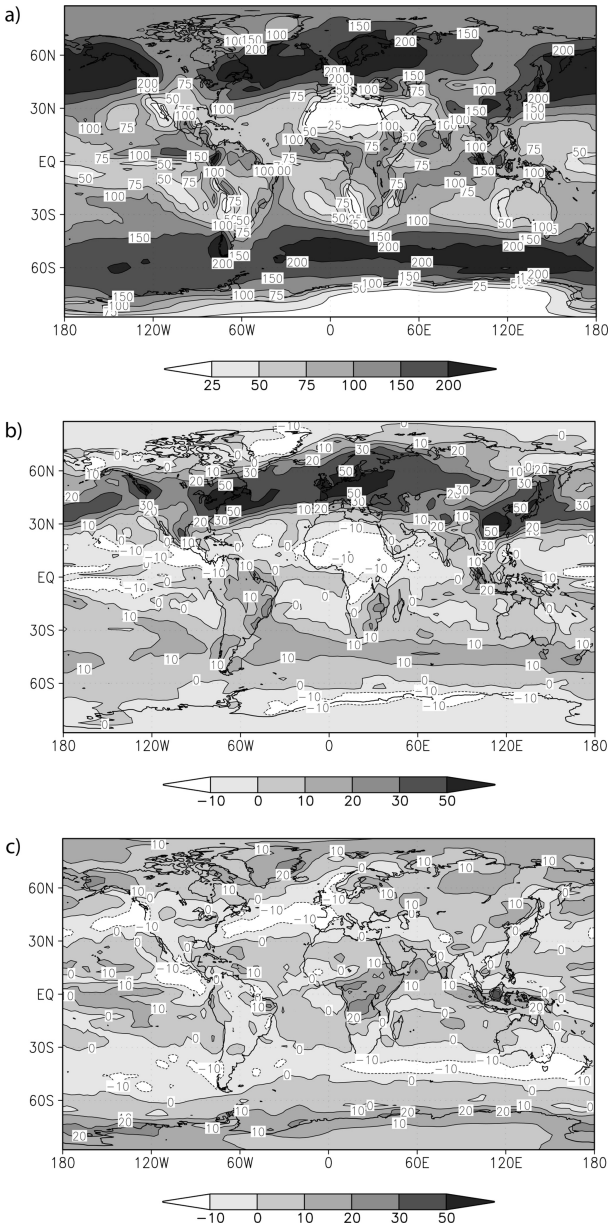

Fig. 6. Column integrated liquid water path (LWP, g m^{-2}): (a) LWP in the control simulation (somB). (b) Change in LWP due to anthropogenic aerosols (somB minus somPre), (c) Change in LWP due to a 63% increase in CO_2 (somBco2 minus somB).

scheme closure assumptions in the host model (Hack et al., 2006).

The simulated global LWCF of 29.4 W m^{-2} (Table 4) is slightly low compared to the 30.4 W m^{-2} in ERBE, see Fig. 7b, and the 30.7 W m^{-2} in CAM3 (Collins et al., 2006a), see Table 3. Regions where we obtain higher LWCF than ERBE are also found, for example, over the western Indian Ocean and parts of the northern Pacific and Atlantic Oceans, similar to what is found in CAM3.

Table 4. Global and hemispheric annual mean cloud forcings at the top of the atmosphere (TOA), as well as albedo, calculated for all-sky conditions. SWCF is short-wave cloud forcing, LWCF is long-wave cloud forcing, and CF is the total cloud forcing, SWCF + LWCF. The cloud forcing data are taken from the last 6 years of the simulations.

	SWCF (W m^{-2})	LWCF (W m^{-2})	CF (W m^{-2})	TOA Albedo (%)	Surface Albedo (%)
somPre					
Global	−51.64	29.96	−21.68	31.4	12.4
NH	−51.15	31.58	−19.57	31.9	13.6
SH	−52.13	28.34	−23.79	31.0	11.2
somB					
Global	−53.70	29.39	−24.31	32.5	13.1
NH	−53.50	30.10	−23.40	33.3	14.6
SH	−53.91	28.69	−25.22	31.7	11.6
somBco2					
Global	−54.00	29.47	−24.54	32.1	12.4
NH	−53.96	30.14	−23.82	32.9	13.9
SH	−54.04	28.79	−25.25	31.4	11.0

4.3. Global and regional climate responses to anthropogenic aerosols and CO_2

In simulation somB minus somPre, the climate responds to anthropogenic aerosol forcing by producing a near global surface cooling of 1.94 K and a 5.5% decrease in precipitation, see Table 2. In Kristjánsson et al. (2005), using CCM-Oslo, anthropogenic aerosols were found to give a somewhat weaker cooling of about 1.44 K, and a 4.4% decrease in the precipitation. However, the main features of the regional surface air temperature response are qualitatively the same as in that work, that is, a strong cooling at high-latitudes, with the largest values found over land in the NH. A much weaker cooling is found over tropical oceans, see Fig. 8a.

The main features of the precipitation responses are also quite similar to those in CCM-Oslo. Apart from the stronger signals in most regions, the largest differences from CCM-Oslo are found in the tropics and subtropics. Over parts of the Indian Ocean south of the equator and over the most of Australia the precipitation signal is reversed compared to CCM-Oslo, as is also the case over northern Africa north of about 15–20°N and over parts of the tropical Pacific Ocean. For the latter region the same reversal was found in equilibrium simulations (not published) with a more recent version of CCM-Oslo where POM was included in addition to sulphate and BC, but with the same aerosol emissions as in CAM-Oslo (Kirkevåg et al., 2005; Kinne et al., 2006; Textor et al., 2006; Schulz et al., 2006). This reversal is therefore probably caused by the relatively large changes in the aerosol distributions and physical properties from the earlier CCM-Oslo version, for example yielding a less clean-cut southward shift of the ITCZ in CAM-Oslo. The same applies to the subtropical

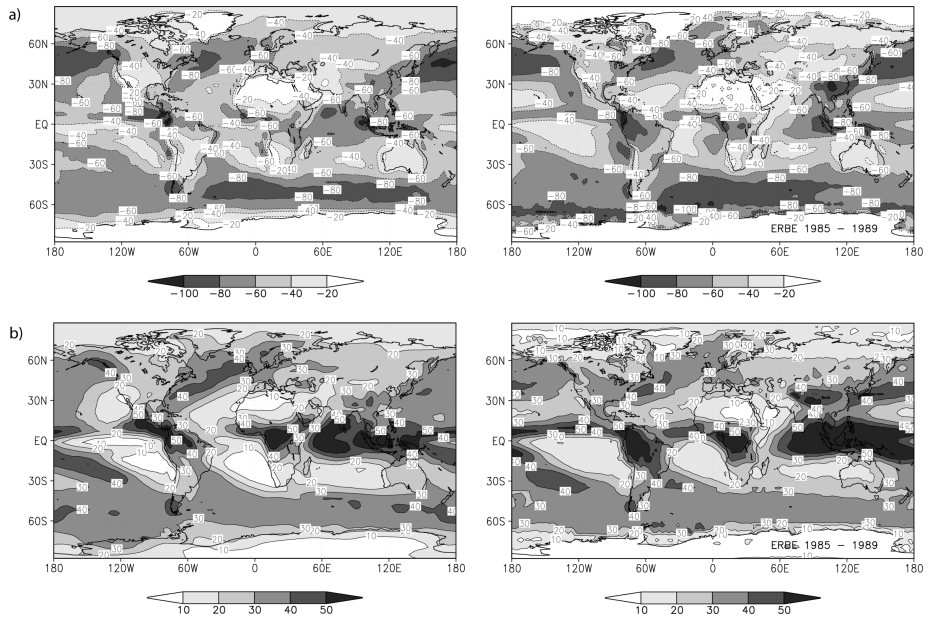

Fig. 7. Cloud forcings (W m^{-2}) in the control simulation somB to the left, and from the Earth Radiation Budget Experiment (ERBE, 1985 – 1989) data to the right. (a) Short-wave cloud forcing (SWCF), (b) Long-wave cloud forcing (LWCF).

Indian Ocean region stretching south-eastwards from Madagascar. For the mentioned areas in northern Africa, central to western parts of Australia and over the Indian Ocean off the Australian west coast, however, the precipitation signal is reversed also relative to the more recent CCM-Oslo version. Although the relative decrease in precipitation is more than 10% over some areas off the Australian west coast, the absolute reduction is nowhere larger than about 0.7 mm day^{-1}. The largest decrease over Northern Africa is about 1 mm day^{-1} (∼90%) over Sahara, and up to about 2 mm day^{-1} (∼50%) in eastern parts of Sudan. These are also the two continental regions with the largest drying due to aerosols in our simulations. Compared to the precipitation response in northern Africa from the indirect effect of sulphate in Rotstayn and Lohmann (2002), the signal is much more similar in the CCM-Oslo version without POM (Kristjánsson et al., 2005) than in CAM-Oslo, where the maximum drying is shifted northwards compared to the two other studies. The signal over Australia (in CAM-Oslo) is more in line with Feichter et al. (2005), where the response to aerosols (including POM) since pre-industrial time is 1–2 mm day^{-1} decrease in precipitation in limited areas.

The 63% increase in CO_2 from somB to somBco2 results in a 1.98 K warming and 3.8% increase in precipitation, globally averaged. The main features of the response in surface air temperature and precipitation in Fig. 8b are similar to what was found for a doubling of CO_2 in Kirkevåg et al. (2008). However, there are large regional differences also here. The most important differences are found in the same areas as discussed for the effect of aerosols, that is northern Africa (about 20°N) and central to western parts of Australia, stretching into the western subtropical Indian Ocean. In Kirkevåg et al. (2008) the response to doubled CO_2, especially in the latter region, was very different in simulations with natural compared to present-day aerosol emissions. With natural aerosols, the precipitation actually increased in this region, very similar to the response in CAM-Oslo for present-day aerosols. This indicates that the regional aerosol-cloud-climate feedbacks affect not only the temperature responses, as discussed in Kirkevåg et al. (2008), but also the precipitation. One additional region with different response in precipitation is found in central to southern Africa, where CAM-Oslo yields an increase (exceeding 10% in some areas), and CCM-Oslo produces a weak decrease (less than about 10%). Also in this region the response to a doubling of CO_2 was found to depend on the aerosol emissions in Kirkevåg et al. (2008).

Estimated combined effects of anthropogenic aerosols and the 63% increase in CO_2 on climate (simulations somBco2 minus somPre) are shown in Fig. 8c. Despite a slight global surface air warming of 0.04 K, we find a more than 1 K cooling over continents at mid and high-latitudes in the NH. Since aerosol emissions are projected to decrease towards the end of the century, the somBco2 simulation may not be realistic as a future scenario. Nevertheless, this result falls outside the range of likely temperature change towards year 2100 in IPCC (2007). In light of observed temperature increase over continents in the NH since pre-industrial time, for which the increase in CO_2 is only about half of that applied here, these simulations indicate that the aerosol cooling is exaggerated in CAM-Oslo, just as concluded for CCM-Oslo (Kristjánsson et al., 2005; Kirkevåg et al., 2008). This issue is discussed in more detail in Section 4.6. Looking at the precipitation response to the combined effects of

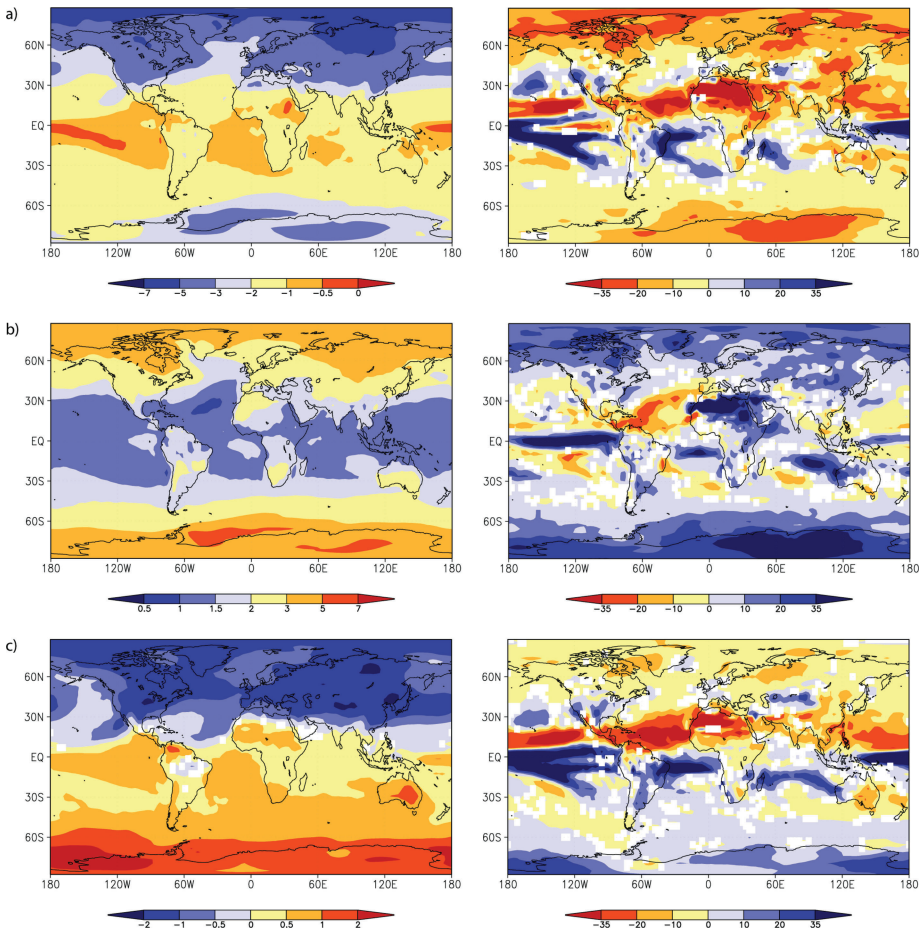

Fig. 8. Changes in surface air temperature (K) (left) and precipitation (%) (right), due to: (a) Joint aerosol direct and indirect effect (somB minus somPre), (b) 63% increase in CO_2 mass mixing ratios (somBco2 minus somB), (c) Joint aerosol direct and indirect effect and 63% increase in CO_2 (somBco2 minus somPre).

anthropogenic aerosols and increased CO_2, the signals over southern Europe, larger parts of Africa, and in several tropical regions in general, seems to agree with observed trends during the 20'th century (IPCC, 2001). Due to the exaggerated effect of aerosols, however, the precipitation decreases where observations indicate an increase both in Australia and over large continental areas at high latitudes in the NH.

Interestingly, while the temperature response from simulation somPre to somBco2 of about 0.05 K is slightly positive, the global precipitation decreases with about 2%, corresponding to a very large so-called hydrological sensitivity (Feichter et al., 2004) of -40% K^{-1}. While this joint hydrological sensitivity to anthropogenic aerosols and a CO_2 doubling was only slightly positive in CCM-Oslo, 0.3% K^{-1} (Kirkevåg et al., 2008), Feichter et al. (2004) also found a negative hydrological sensitivity to changes in aerosols and CO_2 (from pre-industrial to present-day levels), amounting to about -2% K^{-1}. This was mainly a result of an almost three times higher hydrological sensitivity to aerosols (3.9% K^{-1}) than to CO_2 (1.5% K^{-1}). In CAM-Oslo it is estimated at 2.8% K^{-1} for aerosols and 1.9% K^{-1} for CO_2 (see Table 2), quite close to the respective 3.0% K^{-1} and 1.8% K^{-1} found in CCM-Oslo. Hence, the very large hydrological sensitivity in CAM-Oslo does not seem to result as much from any inherent model-dependent sensitivity, as from a 'lucky' combination of anthropogenic aerosol and CO_2 levels, which in this case gives almost no change in the global surface air temperature.

4.4. *Climate feedbacks on aerosol burdens, optical depths and cloud droplet numbers*

Climate change in terms of temperature, humidity, cloud cover, precipitation and prevailing winds feed back on the spatial and temporal distribution of aerosols in the atmosphere. Regionally, the result of these feedbacks is most evident in the simulations with increased CO_2 mass mixing ratio while the emissions of aerosols have been kept unchanged, see Fig. 1c. The simulated burdens for all aerosol components drop considerably at high

Table 5. Global annual mean sources, burdens, lifetimes and wet depositions (% of total deposition) for all species, and chemical loss (% of total loss) for the gas species (cf. SIKS). The numbers in brackets show loss by conversion of Dimethyl Sulphide (DMS) to Methane Sulphonic Acid (MSA), and through wet phase chemistry (% of total chemical loss) for SO_2. Burdens for Sulphur species are given as Tg S.

Species	Experiment	Total Sources (Tg yr^{-1})	Burden (Tg)	Lifetime (days)	Wet deposition (%)	Chemical loss (%)
DMS	somPre	18.0	0.107	2.16		100 (23.5)
	somB	18.1	0.104	2.11		100 (24.8)
	somBco2	18.0	0.108	2.19		100 (23.3)
MSA	somPre	4.25	0.019	1.63	73.9	0
	somB	4.47	0.019	1.58	73.5	0
	somBco2	4.20	0.019	1.68	73.8	0
SO_2	somPre	28.7	0.083	1.06	10.0	81.0 (87.3)
	somB	82.3	0.295	1.31	9.6	71.0 (85.0)
	somBco2	82.5	0.300	1.33	9.2	71.4 (85.0)
Sulphate	somPre	23.6	0.217	3.35	94.1	
	somB	60.4	0.629	3.81	93.0	
	somBco2	60.7	0.626	3.76	93.1	
BC	somPre	1.40	0.026	6.83	81.7	
	somB	7.67	0.142	6.74	75.6	
	somBco2	7.66	0.140	6.64	75.9	
POM	somPre	33.1	0.631	6.95	81.5	
	somB	65.6	1.30	7.23	80.8	
	somBco2	65.5	1.28	7.14	81.1	
Sea-salt	somPre	7708	5.23	0.25	27.0	
	somB	7710	5.40	0.26	26.8	
	somBco2	7709	5.26	0.25	26.4	
Dust	somPre	1669	9.41	2.06	40.0	
	somB	1671	10.06	2.20	37.3	
	somBco2	1670	10.14	2.22	37.9	

latitudes (up to 10–15% for dust and sea-salt), where the burdens are quite small, while there are more complex signals (up to about $\pm 5\%$) at mid-latitudes and in the tropics, where the largest contributions to the aerosol burdens listed in Table 1 are found.

Globally averaged we find modest reductions in sulphate (-0.6%), BC (-1.4%), POM (-1.3%) and sea-salt (-2.6%), and a small increase in the dust burden (0.8%). These are small changes compared to Feichter et al. (2004), where simulated aerosol burdens decreased by as much as 17% K^{-1} warming when the CO_2 levels were increased from pre-industrial to present-day levels. The reductions in aerosol burdens were attributed to a decrease in aerosol life-time due to increased precipitation and shortened cloud life-time. In CCM-Oslo (Kirkevåg et al., 2008), on the other hand, using prescribed sea-salt and dust aerosols, the sulphate and BC burdens were found to increase by about 2 and 3%, respectively. This was possible because of a relatively strong dependence on stratiform precipitation, which was slightly reduced in important source regions, combined with regional reductions in convective precipitation over oceans in the subtropics.

In CAM-Oslo the role of convective precipitation is relatively more important due to the revised treatment of wet scavenging in convective clouds, as well as the fact that the cloud volume in areas with convective precipitation is larger than in CCM-Oslo. For nucleation to accumulation mode sized sulphate, POM and BC, wet scavenging is the dominant deposition process, while for the coarser particles dry deposition dominates (SIKS), see Table 5. Hence, in the warmer somBco2 climate the reduced burdens at high latitudes may to a large extent be ascribed to the relatively large increase in precipitation, causing enhanced wet scavenging and shorter life-times in these regions (as well as globally averaged, see Table 5).

We only find a few percent increase in the deposition of sulphate and dust close to and just north of the equator. For sulphate, this is also reflected in a decrease in burden. However, the dust burden increases and sea-salt is reduced, see Fig. 1c. Looking at the regional distribution of the changes in burden (not shown) at these low latitudes, the strongest decrease in sea-salt near the equator is found over the Pacific ocean, where there is also a marked increase in the precipitation (Fig. 8b) and deposition. The largest increase in dust is found over the African continent south-west of Sahara and further downstream across the Atlantic Ocean as far as into the Caribbean Sea (clearly seen in the AOD in Fig. 2c), where both the precipitation (Fig. 8b) and the dust

deposition are reduced considerably compared to the control simulation. There is a substantial relative increase in dust burdens in the SH subtropics as well (Fig. 1c), but the largest contributions to the increase in global mean burden are found in the NH (see Table 1). A major contribution to the pronounced increase in sulphate at 10–20°N is found over the eastern Pacific Ocean, off the west coast of Central America, while the main source for the spike at 10°S is volcanic activity in the Salomon Islands and New Guinea (both clearly visible in Fig. 2c). Volcanic emissions are important sources in the former case as well, but there we also find a large anthropogenic contribution from Central and North America. In both these regions the precipitation and the sulphate deposition are reduced in the simulation with increased CO_2. A 5–20% increase in (mainly gas phase) sulphate production also contributes, and off the west coast of Central America we find an easterly to north-easterly shift in the wind of about 1 m s^{-1} in the lower troposphere, indicating also a strengthened transport of sulphate from Central and North-America.

AOD depends not only on aerosol burdens but also on aerosol size and composition, as well as on the ambient relative humidity. Some of the increase in AOD in the tropics in Fig. 2c comes from increased hygroscopic growth, since there is an increase in the relative humidity in the lowest 2–3 km by about 2–4% from the somB to the somBco2 simulation, see Fig. 4c. Similarly, some of the decrease in AOD in the extratropics may be explained by a small decrease (less than 2%) in relative humidity at most heights.

The largest increase in simulated CDNC are found at about 5 km height at about 30°S and 40°N (10–50 cm^{-3}) and in the lowest 2–3 km of 40–70°N (10–25 cm^{-3}), see Fig. 3c. In the latter case the increase in the aerosol number concentration is somewhat smaller than the increase in CDNC, and in the former case we actually find a decrease in the aerosol number. An important contribution to the enhanced CDNC is therefore probably the increased convective activity in the warmer climate, giving higher supersaturations than in the present-day simulations. The largest changes in cloud droplet effective radii, however, are found at about 5 km height in the tropics and throughout the SH lower troposphere at mid- to high latitudes. This may to a large degree be explained by the changes in LWC, which increases considerably (exceeding 20% in the tropics at 5 km height) in the mentioned areas of increased R_{effl}, and decreases in much of the tropical middle troposphere (by more than 20% at 3–5 km height) and in a branch of decreased R_{effl} stretching down- and southward at mid-latitudes of the SH. The location of the local maximum for increase in R_{effl} in the lower tropical troposphere is also where the LWC increases the most (exceeding 50%).

Corresponding climate feedbacks on aerosol burdens, AOD and CDNC due to aerosol-induced changes in climate from pre-industrial time to the present are not so straightforward to see from Figs. 1b and 2b, due to the large increase in aerosol emissions from somPre to somB. However, since CDNC increase in the SH, although less than in the NH, the increase in R_{effl} in the middle to lower troposphere in the SH is clearly due to increased LWC. The LWC is larger by about 10–50% in these regions. This is also reflected in a moderate increase in vertically integrated LWC (i.e. the LWP) in Fig. 6b.

Table 6. Experiments with CAM-Oslo run as an atmospheric GCM, testing the sensitivity to background droplet number concentrations (CDNC) and to using prognostic rather than diagnostic CDNC (Storelvmo et al., 2006b). Changes in liquid water path (LWP), effective cloud droplet radii as seen from satellite (R_{effl-S}: as in Kristjánsson, 2002), as well as the combined first and second indirect forcing by anthropogenic aerosols (since pre-industrial time) are global annual means.

CDNC treatment	LWP ($g\ m^{-2}$)	R_{effl-S} (μm)	$1^{st} + 2^{nd}$ Indirect forcing ($W\ m^{-2}$)
Standard CDNC	9.25	−1.41	−2.34
Standard CDNC + 15 cm^{-3}	5.09	−0.99	−1.36
Prognostic CDNC	4.20	−1.00	−1.44

4.5. *Cloud feedbacks and climate sensitivity*

Compared to a 2.6 K warming and 4.8% increase in the precipitation for a doubling of the CO_2 in CCM-Oslo (Kirkevåg et al., 2008), CAM-Oslo yields only a slightly weaker warming (about 2.4 K) and increase in precipitation (about 4.7%) if we assume that the amplitude of the signals increase linearly with an increase in CO_2 mass mixing ratio. The corresponding responses in surface air temperature in CAM2 and CAM3 are 2.27 and 2.47 K, respectively (Kiehl et al., 2006). Although smaller than the best estimate of 3 K in IPCC (2007), all these lie within the given range of likely climate sensitivities of 2 to 4.5 K. Cloud feedbacks remain the largest source of uncertainty.

For the climate response to anthropogenic aerosols, largely through their effect on clouds, the simulated global cooling and drying in CAM-Oslo are larger than in CCM-Oslo by about 35 and 25%, respectively. How is this relatively strong increase in climate response to anthropogenic aerosols related to the radiative forcing? First of all, based only on the change in the direct forcing we should expect a weaker cooling in CAM-Oslo, since the TOA direct forcing here is slightly positive, 0.03 W m^{-2} (SIKS), compared to −0.11 W m^{-2} in CCM-Oslo (Kirkevåg and Iversen, 2002). The first indirect forcing, however, is in CAM-Oslo estimated at −1.78 W m^{-2}, compared to −1.3 W m^{-2} in CCM-Oslo (Kristjánsson, 2002). In a separate test simulation with CAM-Oslo set up as an atmospheric GCM and where also the second indirect effect is calculated as a forcing (cf. Kristjánsson, 2002), the joint first and second indirect effect is estimated at −2.34 W m^{-2}, see Table 6. This is about 28% larger than in CCM-Oslo (−1.83 W m^{-2}). Adding up the direct

and indirect contributions, we find that the short-wave radiative forcing by aerosols in CAM-Oslo is about 19% larger than in CCM-Oslo. Assuming that CCM-Oslo and CAM-Oslo has about the same climate sensitivity, as indicated by the very similar responses to (equal) changes in CO_2, the changes in aerosol forcing thus explains about half of the difference in temperature response.

Comparing Fig. 6 and Table 2 with Kristjánsson et al. (2005), we find considerably larger anthropogenic changes in LWP in the present study: Globally averaged it is here estimated at 7.4 g m^{-2} (7.0%), compared to only -0.15 g m^{-2} (-0.4%) in CCM-Oslo. Despite regionally large increases in LWP over and downstream of industrial emission areas also in CCM-Oslo, a general thinning of the clouds due to the cooling resulted in the negative response, globally averaged. We should also note that LWP in the control simulation with CAM-Oslo is about twice the amount in CCM-Oslo, reflecting the increase in LWP from CCM3 to CAM3. The total cloud water path response of 8.5 g m^{-2} (7.0%) in the present work is in fact much closer to the 8.7 g m^{-2} (10%) obtained by Feichter et al. (2004). For the IWP response, CAM-Oslo yields about 1.1 g m^{-2} (7.4%) increase due to aerosols, compared to 0.06 g m^{-2} (0.3%) in CCM-Oslo.

To establish whether some of the difference can be explained by feedback mechanisms, we may look at how the globally averaged change in cloud forcing (SWCF + LWCF) due to anthropogenic aerosols evolves with time. While in CCM-Oslo there is a considerable drop in strength from about -1.83 W m^{-2} initially (1st + 2nd indirect radiative forcing) to -1.27 W m^{-2} in the last 6 years of the simulations, we find a corresponding increase in strength from about -2.34 to -2.63 W m^{-2} (Table 4) in CAM-Oslo. This positive cloud feedback stands in contrast to the substantial negative feedback in CCM-Oslo (Kristjánsson et al., 2005), and is probably accountable for much of the difference in temperature responses in the two model versions.

4.6. *Sensitivity to uncertain assumptions*

As demonstrated by Lohmann et al. (2000) and SIKS, smaller background aerosol number concentrations (and CDNC) in pristine conditions lead to stronger indirect effects, given the same anthropogenic aerosol emissions. Both of the indirect effects we consider are sensitive to the pristine aerosol number concentrations. In the Rasch and Kristjánsson (1998) scheme for prognostic cloud water there are two processes which control the release of precipitation in warm clouds. The first describes the autoconversion (i.e. collisions and coalescence among cloud droplets) of cloud water to rain, while the other describes the collection of cloud water by rain or snow from above. The autoconversion term, P, has an explicit dependency on CDNC. Assuming that the LWC is constant and the effective cloud droplet radius remains larger than the autoconversion threshold of 15 μm, the sensitivity of P to changes in CDNC may be expressed mathematically as:

$$\frac{\Delta P}{P} = -\frac{1}{3}\frac{\Delta CDNC}{CDNC}.$$

This means that a relative decrease in precipitation will tend to be comparatively large (for a given anthropogenic aerosol concentration) where the relative increase in CDNC is large, such as over naturally pristine ocean or continental regions. The sensitivity becomes even larger in areas where also the typical effective cloud droplet radii are close to the autoconversion threshold radius, since smaller droplets are unable to produce rain through the autoconversion process. Consequently, the second indirect effect (through a response in the LWC) is comparatively large in these areas. For the first indirect effect the sensitivity of the cloud albedo, A, to changes in cloud droplet effective radii, R_{eff}, that is the so-called cloud susceptibility, may be expressed as (Twomey, 1991):

$$\Delta A = -A(1-A)\frac{\Delta R_{eff}}{R_{eff}} = \frac{1}{3}A(1-A)\frac{\Delta CDNC}{CDNC}.$$

Hence, the first indirect effect will be comparatively large where the relative increase in CDNC is large (and where the cloud albedo is close to 0.5). Here, we should also note that the first indirect effect is probably somewhat limited in strength by the use of the prescribed lower and upper limits of 4 and 20 μm for R_{eff} in the Slingo (1989) scheme for short-wave radiative properties of cloud droplets in CAM3.

In CCM-Oslo the CDNC in pristine conditions has a relatively high lower cut-off, due to the much higher background (sea-salt, mineral and water soluble continental) aerosol number concentrations (Kirkevåg, 2002; Kristjánsson 2002) than in the present model study. In the absence of Aitken mode-sized sulphate, BC and POM aerosols (introduced in CAM-Oslo), background aerosol number concentrations were prescribed to rather high values in order to obtain reasonable total aerosol number concentrations compared with observations. The prescribed aerosol number concentrations in CCM-Oslo also had less temporal variability than the fully prognostic aerosols in CAM-Oslo, which are modelled from natural and anthropogenic emissions of aerosol and aerosol precursors, see SIKS.

To test whether the large indirect effect in CAM-Oslo in large parts may be due to the much lower background aerosol number concentrations than in CCM-Oslo and many other global models (e.g. Rotstayn and Lohmann, 2002, where CDNC $>$ 114.8 cm^{-3} everywhere), we have run two additional offline simulations with CAM-Oslo set up as an atmospheric GCM, one with pre-industrial and one with present-day aerosol emissions. In both these simulations we increase CDNC by 15 cm^{-3} everywhere, relative to the standard simulations. Thus, the anthropogenic CDNC are still as in the standard simulations. With pristine CDNC more similar to those in CCM-Oslo over ocean, but still much lower than CCM-Oslo over land, this gives a combined first and second indirect effect of -1.36 W m^{-2}, compared to -2.34 W m^{-2} in the control simulations, that is a 42%

smaller indirect effect. The anthropogenic change in LWP and effective cloud droplet radius as seen from satellite (following Kristjánsson, 2002) are as much as 45% and 30% lower when the natural CDNC are increased by 15 cm^{-3}.

Another important contributing factor to the large indirect effect may be associated with the use of prescribed supersaturations for CCN activation. Using a prognostic equation for CDNC (and supersaturations based on a subgrid distribution of vertical velocities) in a preliminary CAM-Oslo version based on NCAR CAM2 and aerosol modules from CCM-Oslo, Storelvmo et al. (2006b) obtained a considerably smaller aerosol indirect forcing. Quite recently an adapted version of this scheme for prognostic CDNC has been implemented also in the new (present) CAM-Oslo version. A separate sensitivity test run to quantify the effect of this improvement, yield an important reduction of the indirect forcing from -2.34 W m^{-2} to -1.44 W m^{-2}. Table 6 summarizes the results from the test simulations.

Based on these tests, our hypothesis is that the relatively large indirect effect in the present work, both in terms of radiative forcing and climate response, is related to the small CDNC for pristine conditions in CAM-Oslo as well as the assumption of presumed supersaturations. Missing aerosol components of natural as well as anthropogenic origins in CAM-Oslo (as well as other atmospheric GCMs) include particulate nitrate and biological particles (e.g. Jaenicke, 2005).

5. Summary and conclusions

Equilibrium climate responses to anthropogenic aerosols and increased CO_2 levels have been investigated based on three multi-decadal simulations with CAM-Oslo (SIKS) coupled to a slab ocean model. CAM-Oslo is a modified version of the global climate model NCAR CAM3. Its aerosol module interacts fully with the meteorology through a life-cycle scheme for sea-salt, mineral, sulphate, BC and POM, which is coupled to calculations of aerosol optical parameters and CDNC by use of pre-calculated look-up tables. The basic assumptions underlying the look-up tables and the life-cycle module are to a large extent internally consistent. For example, cloud droplet effective radii with respect to scattering of light and release of precipitation through autoconversion are intimately interconnected, and the AOD cannot be tuned without modifying the aerosol life cycle scheme, thus also affecting the number and size of cloud droplets.

Using present-day aerosol emissions and CO_2 levels, CAM-Oslo is shown to simulate climate well with respect to cloud cover, cloud liquid water, cloud radiative forcing and energy fluxes at the ground surface. A warm bias in the surface air temperature of about 1 K globally could have been reduced (and will be, in future work) by using CAM-Oslo itself, instead of the original CAM3, in the calibration of the ocean heat transport fluxes in the slab ocean model. Due to this warm bias the precipitation rate is somewhat overestimated, and the polar sea-ice area is too small.

A 63% increase in CO_2 gives a 2.0 K global mean surface air warming and a 3.8% increase in precipitation, when present-day aerosol emissions are used. This corresponds to a temperature response of approximately 2.4 K for a doubling of CO_2, which is somewhat lower than the most probable value of 3 K given in IPCC (2007), but well within the range of likely equilibrium climate sensitivities of 2–4.5 K. It is also quite similar to what was found in CCM-Oslo, the predecessor of CAM-Oslo. The CO_2-induced changes in climate in terms of circulation, clouds, and precipitation patterns feed back on the spatial and temporal distribution of aerosols, causing modest global reductions in burdens of sulphate (-0.6%), BC (-1.4%), POM (-1.3%) and sea-salt (-2.6%), but a small increase in the dust burden (0.8%). All burdens are substantially reduced at high latitudes due to increased precipitation and deposition, while at lower latitudes there are mixed results, including increased as well as decreased burdens. The main contribution to the net increase in the global dust burden is a substantial increase downwind of Sahara and western Africa, stretching across the Atlantic Ocean where both precipitation and deposition are reduced in this scenario.

The total net effects of anthropogenic aerosols compared to pre-industrial time produce a global 1.9 K surface air cooling and a 5.5% decrease in precipitation. As in earlier studies, the strongest cooling takes place in the NH, giving rise to a southward shift of the ITCZ. The equilibrium responses in surface air temperature and precipitation in CAM-Oslo are larger than in CCM-Oslo by as much as 35% and 25%, respectively, while the joint direct and indirect radiative forcing by aerosols (at TOA) is only 19% larger. Parts of this can be attributed to a positive cloud feedback, enhancing the climate response in CAM-Oslo. In CCM-Oslo (Kristjánsson et al., 2005) a similar negative feedback damping the signal was found.

Since the background, that is natural and pristine, number concentrations of aerosols and cloud droplets are considerably smaller in CAM-Oslo than in CCM-Oslo, we have run experiments with CAM-Oslo as a pure atmospheric GCM in order to quantify how sensitive the indirect effect is to these background aerosol numbers. With standard CDNC we estimate a joint 1st and 2nd indirect effect of -2.34 W m^{-2}, while a prescribed modest increase in background CDNC of 15 cm^{-3} added everywhere, causes a 42% reduction to only -1.36 W m^{-2}. This result is in agreement with Lohmann et al. (2000), as well as with tests of the sensitivity of the 1st indirect effect to sea-salt aerosol number concentrations in Seland et al. (2008). The result emphasizes the importance of a realistic modelling of natural aerosols, since the same anthropogenic aerosol emissions cause considerably different forcing and climate response just by a slight change in the background aerosol which determines the minimum number of cloud droplets (cf. Lohmann and Feichter, 2005). Similar reductions in the forcing by the indirect effects (from -2.34 W m^{-2} to -1.44 W m^{-2}) are obtained by improving the modelling of cloud droplet number as in Storelvmo et al. (2006b).

Implementation and further development of the prognostic cloud droplet number scheme in the present CAM-Oslo is underway. There are also plans to include effects of aerosols on cold clouds, which potentially have a large impact on the hydrological cycle, and may partly counteract the cloud lifetime effect in warm clouds (Lohmann and Feichter, 2005). Changes in albedo due to deposition of BC on sea-ice and snow is also an effect which is planned to be accounted for in future work.

Results for dynamical downscaling of the somB and somBco2 simulations are described in Haugen and Iversen (2008).

6. Acknowledgments

This study was supported by the Norwegian Research Council through the RegClim and AerOzClim projects, and partly through the NorClim project in 2007. Furthermore, the work has received support of the Norwegian Research Council's Programme for Supercomputing through a grant of computer time. We gratefully acknowledge P. J. Rasch and S. Ghan for sharing code and scientific advice under the development of CAM-Oslo.

7. Appendix

A minor inaccuracy in the code that generates the optics and CCN lookup-tables in SIKS was discovered after submission of the revised version of this paper. Preliminary corrected re-calculations only show small impacts of the inaccuracy, and we have chosen to present the original simulations. The corrected look-up tables changed the calculated global TOA direct radiative forcing from 0.04 to 0.03 W m^{-2} and the global TOA first indirect radiative forcing from -1.76 to -1.78 W m^{-2}. We have not had time to re-calculate for the second indirect forcing (Table 6).

The multi-decadal simulations presented in the main text of this paper are based on the slightly inaccurate version of the look-up tables. By comparing with the sensitivity tests in SIKS, we are confident that the effect of the inaccuracy on the aerosol radiative forcing is considerably smaller than the effects of uncertainties in the aerosol treatment, which are present in state-of-the-art aerosol-climate models. A re-run of the multi-decadal simulations with corrected look-up tables was just recently finished. The corrected simulations of somB and somPre (see Section 3 for definitions) yielded only small changes in global near surface temperature and precipitation: a 2.09 K cooling and a 5.8% decrease in precipitation, compared to 1.94 K and 5.5% originally. The corrected simulations of varying CO_2 (simulation somBco2 and somB) give even smaller changes: a 1.99 K warming and a 3.8% increase in precipitation, compared to 1.98 K and 3.8% respectively.

The changes may be larger in some regions. The most important regional changes in the climate response to anthropogenic aerosols is a somewhat stronger and more widespread increase in precipitation in southern Europe (near the Mediterranean), as well as a shift from a slight increase to a slight decrease in precipitation over central parts of Australia. The corrected results for these two cases are more similar to the responses found with CCM-Oslo (Kirkevåg et al., 2008). Global changes in cloud water path due to anthropogenic aerosols and CO_2 are found to be almost unchanged compared to the original simulations, which implies negligible changes in the second indirect effect. The response in LWP from simulation somPre to somB is 7.1% instead of 7.0%, and from simulation somB to somBco2 it is estimated at 1.4% in both cases.

Another point worth mentioning is that the global surface air temperature in simulation somBco2 becomes slightly lower than somPre, rather than being slightly higher (i.e. -0.1 K instead of $+0.05$ K, see Table 2), while the difference in precipitation is almost unchanged. Hence, the combined hydrological sensitivity to anthropogenic aerosols and a 63% increase in CO_2 becomes $+20\%$ K^{-1} instead of -40% K^{-1}. This strengthens our conclusion in Section 4.3, that the large hydrological sensitivity in CAM-Oslo is due to a coincidental combination of anthropogenic aerosol and CO_2 levels in these specific simulations rather than being an inherent model-dependent property. This is because of the very small response in the global surface air temperature from somPre to somBco2.

The performance of the corrected model in terms of simulation of present day climate is found to be very similar to the original simulations, although the warm bias is reduced by about 0.1 K globally.

References

Abdul-Razzak, H. and Ghan, S. J., 2000. A parameterization of aerosol activation. Part 2: Multiple aerosol types. *J. Geophys. Res.* **105**(D), 6837–6844.

Albrecht, B. A. 1989. Aerosols, cloud microphysics and fractional cloudiness. *Science* **245**, 1227–1230.

Andreae, M. O., Jones, C. D. and Cox, P. M. 2005. Strong present-day aerosol cooling implies a hot future. *Nature* **435**, 1187–1190.

Boer, G. J. and Yu, B., 2003. Climate sensitivity and response. *Climate Dynamics* **20**, 415–429, DOI 10.1007/s00382–002-0283–3.

Boville, B. A., Rasch, P. J., Hack, J. J. and McCaa, J. R. 2006. Representation of clouds and precipitation prcosesses in the Community Atmosphere Model Version 3 (CAM3). *J. Climate* **19**, 2184–2198.

Briegleb, B. P., Bitz, C. M., Hunke, E. C., Lipscomb, W. H., Holland, M. M. and co-authors. 2004. *Scientific description of the sea ice component in the Community Climate System Model, Version Three*. Tech. Rep. NCAR/TN-463+STR, National Center for Atmospheric Research, Boulder, CO, 78 pp.

Cakmur, R. V., Miller, R. L., Perlwitz, J., Geogdzhayev, I. V., Ginoux, P. and co-authors. 2006. Constraining the magnitude of the global dust cycle by minimizing the difference between a model and observations. *J. Geophys. Res.* **111**, D06207, doi:10.1029/2005JD005791.

Collins, W. D., Rasch, P. J., Boville, B. A., Hack, J. J., McCaa, J. R. and co-authors. 2004. *Description of the NCAR Community Atmosphere*

Model (CAM3). Tech. Rep. NCAR/TN-464+STR, National Center for Atmospheric Research, Boulder, CO, 226 pp.

Collins, W. D., Rasch, P. J., Boville, B. A., Hack, J. J., McCaa, J. R. and co-authors. 2006a. The Formulation and Atmospheric Simulation of the Community Atmospheric Model Version 3 (CAM3). *J. Climate* **19**, 2144–2161.

Collins, W. D., Bitz, C. M., Blackmon, M. L., Bonan, G. B., Bretherton, C. S. and co-authors. 2006b. The Community Climate System Model Version 3 (CCSM3). *J. Climate* **19**, 2122–2143.

Dentener, F., Kinne, S., Bond, T., Boucher, O., Cofala, J. and co-authors. 2006. Emissions of primary aerosols and precursor gases in the years 2000 and 1750 prescribed data-sets for AeroCom. *Atm. Chem. Physics* **6**, 4321–4344.

Feichter, J., Roeckner, E., Lohmann, U. and Liepert, B. 2004. Nonlinear aspects of the climate response to greenhouse gas and aerosol forcing. *J. Climate* **17**, 2384–2398.

Fetterer, F. and Knowles, K. 2002. updated 2006. *Sea Ice Index*. Boulder, CO: National Snow and Ice Data Center. Digital media (http://nsidc.org/data/seaice_index/).

Forster, P., Ramaswamy, V., Artaxo, P., Berntsen, T., Betts, R. and co-authors. 2007. Changes in Atmospheric Constituents and in Radiative Forcing. In: *Climate Change 2007: The Physical Science Basis. Contribution of Working Group I to the Fourth Assessment Report of the Intergovernmental Panel on Climate Change* (Eds Solomon, S., Qin, D., Manning, M., Chen, Z., Marquis, M., Averyt, K. B., Tignor, M. and Miller, H. L.). Cambridge University Press, Cambridge, United Kingdom and New York, NY, USA.

Ghan, S. J., Leung, L. R., Easter, R. C. and Abdul-Razzak, H. 1997. Prediction of cloud droplet number in a general circulation model. *J. Geophys. Res.* **102**, 21,777–21,794.

Ghan, S. J., Guzman, G. and Abdul-Razzak, H., 1998. Competition between sea salt and sulfate particles as cloud condensation nuclei. *J. Atmos. Sci.* **55**, 3340–3347.

Hack, J. J., Caron, J., Yeager, S. G., Pleson, K., Holland, M. and co-authors. 2006. Simulation of the Global Hydrological Cycle in the CCSM Community Atmosphere Model Version 3 (CAM3): Mean features. *J. Climate* **19**, 2199–2221.

Harrison, E. F., Minnis, P., Barkstrom, B. R., Ramanathan, V., Cess, R. D. and co-authors. 1990. Seasonal variation of cloud radiative forcing derived from the Earth Radiation Budget Experiment. *J. Geophys. Res.* **95**, 18687–18703.

Haugen, J. E. and Iversen, T. 2008. Response in extremes of daily precipitation and wind from a downscaled multi-model ensemble of anthropogenic global climate change scenarios. *Tellus* **60A**, doi: 10.1111/j.1600-0870.2008.00315.x .

IPCC, 2001. *Climate Change 2001: The Scientific Basis*. Contribution of Working Group I to the Third Assessment Report of the Intergovernmental Panel on Climate Change (Eds Houghton, J. T., Ding, Y., Griggs, D. J., Noguer, M., van der Linden, P. J., Dai, X., Maskell, K. and Johnson, C. A.). Cambridge University Press, 881 pp.

IPCC, 2007. *Climate Change 2007: The Physical Science Basis. Summary for Policymakers*. Contribution of Working Group I to the Fourth Assessment Report of the Intergovernmental Panel on Climate Change. WMO, Geneva, Switzerland, 18 pp.

Iversen, T., Kristjánsson, J. E., Kirkevåg, A. and Seland, Ø. 2005. Calculated feedback effects of climate change caused by anthropogenic aerosols. *RegClim General Technical Report **No.** **8***, 111–120.

Jaenicke, R., 2005. Abundance of cellular material and proteins in the atmosphere. *Science* **308**, 73.

Kiehl, J. T. and Trenberth, K. E. 1997. Earth's Annual Global Mean Energy Budget. *Bull. Am. Meteorol. Soc.* **78**(2), 197–208.

Kiehl, J. T., Schields, C. A., Hack, J. J. and Collins, W. D. 2006. The climate sensitivity of the Community Climate System Model: CCSM3. *J. Climate* **19**, 2584–2596.

Kinne, S., Schulz, M., Textor, C., Guibert, S., Balkanski, Y. and co-authors. 2006. An AeroCom initial assessment – optical properties in aerosol component modules of global models. *Atm. Chem. Phys.* **6**, 1815–1834.

Kirkevåg, A. and Iversen, T. 2002. Global direct radiative forcing by process-parameterized aerosol optical properties. *J. Geophys. Res.* **107**(D20), 4433, doi:10.1029/2001JD000886.

Kirkevåg, A., Iversen, T., Seland, Ø. and Kristjánsson, J. E. 2005. Revised schemes for aerosol optical parameters and cloud condensation nuclei in CCM-Oslo. *Institute Report Series*, Department of Geosciences, University of Oslo, 29 pp, ISBN 82–91885-31–1, ISSN 1501–6854-128.

Kirkevåg, A., Iversen, T., Kristjánsson, J. E., Seland, Ø. and Debernard, J. B. 2008. On the additivity of climate response to anthropogenic aerosols and CO_2, and the enhancement of future global warming by carbonaceous aerosols. *Tellus* **60A**, doi: 10.1111/j.1600-0870.2008.00308.x.

Kristjánsson, J. E. 2002. Studies of the aerosol indirect effect from sulfate and black carbon aerosols. *J. Geophys. Res.* **107**(D15), 4246, doi:10.1029/2001JD000887.

Kristjánsson, J. E., Iversen, T., Kirkevåg, A., Seland, Ø. and Debernard, J. 2005. Response of the climate system to aerosol direct and indirect forcing: Role of cloud feedbacks. *J. Geophys. Res.* **110**, D24206, doi:10.1029/2005JD006299.

Leck, C. and Bigg, E. K., 2007. Comparison of sources and nature of the tropical aerosol with the summer high Arctic aerosol. *Tellus B*, doi: 10.1111/j.1600–0889.2007.00315.x.

Legates, D. R. and Willmott, C. J. 1990. Mean seasonal and spatial variability in global surface air temperature. *Theor. Appl. Climatol.* **41**, 11–21.

Levitus, S., 1982. *Climatological Atlas of the World Ocean*. NOAA Professional Paper 13, National Oceanic and Atmospheric Administration, 173 pp.

Lohmann, U. and Lesins, G., 2002. Stronger Constraints on the Anthropogenic Indirect Aerosol Effect. *Science* **298**, 1012–1015.

Lohmann, U. and Feichter, J. 2005. Global indirect aerosol effects: a review. *Atmos. Chem. Phys.* **5**, 715–737.

Lohmann, U., Feichter, J., Penner, J. E. and Leaitch, W. R. 2000. Indirect effect of sulfate and carbonaceous aerosols: a mechanistic treatment. *J. Geophys. Res.* **105**, 12193–12206.

Lohmann, U., Quaas, J., Kinne, S. and Feichter, J. 2007. Different Approaches for Constraining Global Climate Models of the Anthropogenic Indirect Aerosol Effect. *Bull. Amer. Meteorol. Soc.*, doi:10.1175/BAMS-88–2-243.

Murphy, J. M., Sexton, D., Barnett, D., Jones, G., Webb, M. and co-authors. 2004. Quantification of modelling uncertainties in a large ensemble of climate change simulations. *Nature* **430**, 768–772.

Penner, J. E., Quaas, J., Storelvmo, T., Takemura, T., Boucher, O. and co-authors. 2006. Model intercomparison of indirect aerosol effects. *Atm. Chem. Phys.* **6**, 3391–340.

Pruppacher, H. R. and Klett, J. D., 1997. *Microphysics of clouds and precipitation*. Kluwer Academic Publishers, Dordrecht, 954 pp.

Quaas, J., Boucher, O. and Lohmann, U. 2006. Constraining the total aerosol indirect effect in the LMDZ and ECHAM4 GCMs using MODIS satellite data. *Atmos. Chem. Phys.* **6**, 947–955.

Ramaswamy, V. (co-ordinating lead author), 2001. *Radiative forcing of climate change*. Chapter 6 in the Third Assessment Report of the Intergovernmental Panel on Climate Change. Cambridge University Press, pp. 349–416.

Rasch, P. J. and Kristjánsson, J. E. 1998. A comparison of the CCM3 model climate using diagnosed and predicted condensate parameterizations. *J. Climate* **11**, 1587–1614.

Rossow, W. B. and Dueñas, E. N. 2004. The International Satellite Cloud Climatology Project (ISCCP) Web Site: An online resource for research. *Bull. Am. Meteorol. Soc.* **85**, 167–172.

Rossow, W. B. and Schiffer, R. A. 1999. Advances in understanding clouds from ISCCP. *Bull. Am. Meteorol. Soc.* **80**, 2261–2287.

Rotstayn, L. D., Ryan, B. F. and Penner, J. E. 2000. Precipitation changes in a GCM resulting from the indirect effects of anthropogenic aerosols. *Geophys. Res. Lett.* **27**, 3045–3048.

Rotstayn, L. D. and Lohmann, U. 2002. Tropical rainfall trends and the indirect aerosol effect. *J. Climate* **15,** 2103–2116.

Schulz, M., Textor, C., Kinne, S., Balkanski, Y., Bauer, S. and co-authors. 2006. Radiative forcing by aerosols as derived from the AeroCom present-day and pre-industrial simulations. *Atm. Chem. Phys.* **6**, 5225–5246.

Seland, Ø., Iversen, T., Kirkevåg, A. and Storelvmo, T. 2008. Aerosol-climate interactions in the CAM-Oslo atmospheric GCM and investigation of associated basic shortcomings. *Tellus* **60A**, doi: 10.1111/j.1600-0870.2008.00318.x.

Slingo, A., 1989. A GCM parameterization for the shortwave radiative properties of water clouds. *J. Atmos. Sci.* **46**, 1419–1427.

Stainforth, D. A., Aina, T., Christensen, T., Collins, M., Faull, N. and co-authors. 2005. Uncertainty in predictions of the climate response to rising levels of greenhouse gases. *Nature* **433**, 403–406.

Stier, P., Feichter, J., Kinne, S., Kloster, S., Vignati, E. and co-authors. 2005. The aerosol-climate model ECHAM5-HAM. *Atmos. Chem. Phys.* **5**, 1125–1156.

Stier, P., Feichter, J., Roeckner, E., Kloster, S. and Esch, M., 2006. The evolution of the global aerosol system in a transient climate simulation from 1860 to 2100. *Atmos. Chem. Phys.* **6**, 3059–3076,

Storelvmo, T., Kristjánsson, J. E., Myhre, G., Johnsrud, M. and Stordal, F. 2006a. Combined observational and modeling based study of the aerosol indirect effect (COMBINE). *Atmos. Chem. Phys.* **6**, 3583–3601.

Storelvmo, T., Kristjánsson, J. E., Ghan, S., Kirkevåg, A., Seland, Ø. and Iversen, T. 2006b. Predicting cloud droplet number in CAM-Oslo. *J. Geophys. Res.* **111**, D24208, doi:10.1029/2005JD006300.

Takemura, T., Nozawa, T., Emori, S., Nakajima, T. Y. and Nakajima, T. 2005. Simulation of climate response to aerosol direct and indirect effects with aerosol transport-radiation model. *J. Geophys. Res.* **110**, D02202, doi:10.1029/2004JD005029.

Teng, H., Buja, L. E. and Meehl, G. A. 2006. Twenty-first century climate change commitment from a multi-model ensemble. *Geophys. Res. Lett.* **33**, L07706, doi:10.1029/2005GL024766.

Textor, C., Schulz, M., Guibert, S., Kinne, S., Balkanski, Y. and co-authors. 2006. Analysis and quantification of the diversities of aerosol life cycles within AeroCom. *Atm. Chem. Phys.* **6**, 1777–1813.

Twomey, S. 1977. The influence of pollution on shortwave albedo of clouds. *J. Atmos. Sci.* **34**, 1149–1152.

Twomey, S. 1991. Aerosols, Clouds and Radiation. *Atmos. Environ.* **11**, 2435–2442.

von Storch, H. and Zwiers, F. W. 1999. *Statistical analysis in climate research*. Cambridge University Press, 484 pp.

Williams, K. D., Jones, A., Roberts, D. L., Senior, C. A. and Woodage, M. J. 2001. The response of the climate system to the indirect effects of anthropogenic sulfate aerosol. *Climate Dyn.* **17**, 845–856.